FINAL REPORT

INVERSION LAYER SOLAR CELL FABRICATION AND EVALUATION

JPL Contract No. 953461

September 1973

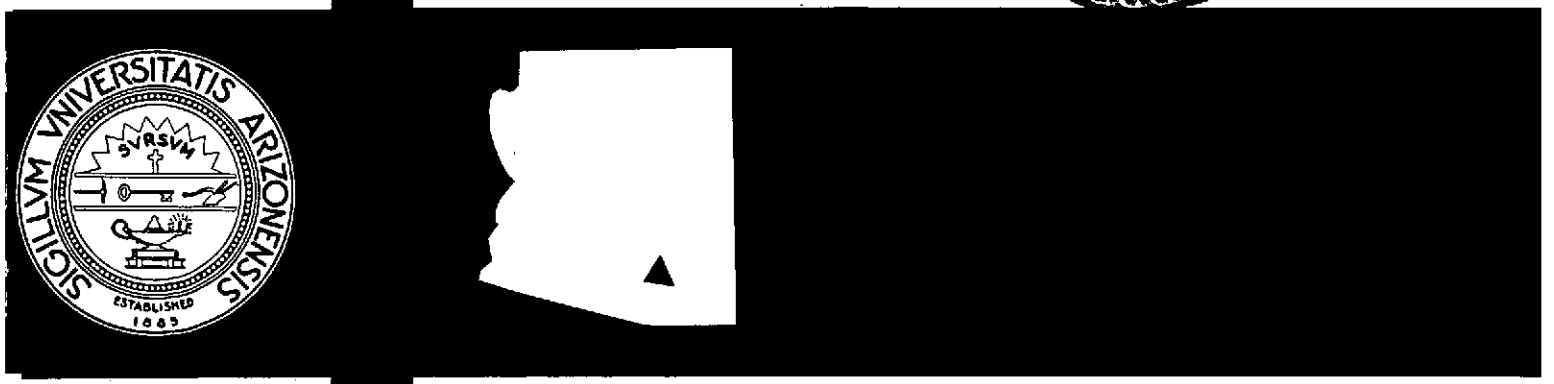

ENGINEERING EXPERIMENT STATION
COLLEGE OF ENGINEERING
THE UNIVERSITY OF ARIZONA
TUCSON, ARIZONA

INVERSION LAYER SOLAR CELL FABRICATION AND EVALUATION

Final Report

by

R. L. Call, Principal Investigator
Electrical Engineering Department
The University of Arizona

September 1973

JPL Contract No. 953461

to

Jet Propulsion Laboratory
California Institute of Technology

This work was performed for the Jet Propulsion Laboratory, California Institute of Technology sponsored by the National Aeronautics and Space Administration under Contract NAS7-100.

TABLE OF CONTENTS

ABSTRACT

Silicon solar cells operating with induced junctions rather than diffused junctions have been fabricated and tested. Induced junctions were created by forming an inversion layer near the surface of the silicon by supplying a sheet of positive charge above the surface. This charged layer was supplied through three mechanisms:

1. applying a positive potential to a transparent electrode separated from the silicon surface by a dielectric,
2. contaminating the oxide layer with positive ions, and
3. forming donor surface states that leave a positive charge on the surface.

A movable semi-infinite shadow delineated the extent of sensitivity of the cell due to the inversion region. Measurements of the response of the inversion layer cell to light of different wavelengths indicated it to be more sensitive to the shorter wavelengths of the sun's spectrum than conventional cells. The greater sensitivity occurs because of the shallow junction and the strong electric field at the surface. Theory of the conductance of the inversion layer vs. strength of the inversion layer was compared with experiment and found to match. Theoretical determinations of junction depth and inversion layer strength was made as a function of the surface potential for the transparent electrode cell.

SUMMARY

This report relates experimental and theoretical work done to demonstrate that an induced junction, formed by creating an inversion layer at the surface of a semiconductor, can be used to separate hole-electron pairs created by photons and thus can be used as a device to convert solar radiation to electrical energy.

The increase in output when the inversion region was induced by a transparent electrode separated by an insulator is described. An opaque knife edge drawn across the face of the cell delineated sensitive portions of the cell and showed the area of sensitivity to increase as the inversion layer grew.

Cells were fabricated by contaminating the oxide layer on the cell with positive ions and thereby inducing an inversion layer in the semiconductor. Results similar to the transparent electrode cell were obtained. A decrease in cell response was found as the oxide was incrementally etched away.

Attempts to fabricate a cell using surface states as the source of positive charge were made and the results reported.

A match of theory vs. experimental results was made between the conductance of the inversion layer and the magnitude of the inversion layer. A study of the inversion region as a p-n junction and its action as a photovoltaic cell was also made.

The V-I characteristic of the inversion layer cells shows a small curve factor and therefore a low efficiency. This is due to a high contact resistance. Attempts were made to make low resistant Ti-Ag contacts, but

these contacts peeled from the silicon surface during the photoetch process. Stable low resistance contacts were made on conventional p-n cells, however, indicating that the deposition and sintering stages were not at fault.

Rough spectral response measurements were made and the inversion layer cell was found to be more sensitive to the shorter wavelengths in the sun's sprectrum than a conventional cell due to the shallower junction and the strong electric field that exists at the surface. A series of narrow band optical filters was used to obtain a comparison between the inversion layer cell and the conventional cell with respect to sensitivity to the short wavelength part of the sun's spectrum.

I. INTRODUCTION

A metallurgical p-n junction with a built-in electric field across the depletion region can act as a collecting medium for hole-electron pairs created by photons. The unlike charges gather on either side of the junction and cause a potential difference across the diode. A current can be extracted from the device at a reasonable potential difference and therefore the device is capable of delivering power to an outside load. Maximum power can be drawn from the diode or photovoltaic cell by adjusting the load for maximum power transfer. Very low internal impedance is needed to minimize the internal power consumption and raise the efficiency of the cell. Figure 1 shows a typical V-I curve for a photovoltaic cell.

If the cell is used to convert the sun's radiation to electrical power, the efficiency will depend on the band gap of the semiconductor with respect to the photon energy spectrum of the sun. The efficiency will also depend on the collection efficiency of the p-n junction, that is, the probability of a hole-electron separation by the field at the depletion region before recombination takes place. The collection efficiency, then, will depend on the distance of the junction from the places of hole-electron creation, as well as the diffusion length of the charge carriers in the semiconductor. A conventional p-n solar cell configuration is found in Fig. 2. The cross section of the device is shown in the drawing with the electric field as shown.

To obtain maximum power from the cell, certain factors arise that require trade-offs to occur. For instance, to obtain a low internal resistance for the n layer, and therefore little internal power loss in this layer, a rather thick layer would be desirable. However, a thick layer

means the junction is located deep below the top surface and hole-electron pairs created at the surface by the short wavelength rays from the sun will have a greater chance of recombining before being collected. Thus, the junction depth is adjusted as a compromise between the two needs.

Another similar adjustment occurs between the need for a heavily doped n layer for low resistance and a lightly doped n layer for long diffusion length. Again considering the plight of the pairs produced at the surface by the short wavelength portion of the sun's spectrum.

Another type of p-n junction exists, however, besides the metallurgical junction. This junction is an induced junction formed by attracting electrons to the surface of a p type semiconductor and converting the surface to n type. In the metallurgical junction the p and the n are created by impurity dopants in the silicon, but in the induced junction the n is created in the p semiconductor by capacitor action. A positively charged layer is formed close to the surface but isolated from it. This positive layer attracts electrons to the surface that fills the holes at the surface until they are all filled and the electrons left over are free electron carriers creating an n layer. A thin layer at the surface has thus been inverted from p to n and is therefore called the inversion layer. This induced p-n junction has a built-in field and a depletion region as has the metallurgical junction. Therefore, this junction should be capable of separating photon produced hole-electron pairs and, therefore, act as a photovoltaic cell or solar cell.

The inversion layer cell has a distinct advantage over the conventional cell, however. Whereas the electric field of the conventional cell exists only at the junction, which might be comparatively deep beneath the

surface so that no field exists at the surface, the field of the inversion layer cell originates outside the surface so the field is maximum at the surface. Thus, free charges created at the surface by ultraviolet photons are found in a high field and their separation aided by the force of the field on the carriers. Therefore, the inversion cell should produce more power from the short wavelength part of the sun's spectrum because more pairs created at the surface are collected before they recombine than in the conventional cell. A cross section of the inversion layer cell is found in Fig. 3. To collect the electrons, it is necessary that n diffusions be connected to the inversion layer as shown.

The p type part of the cell below the junction is the same in both types of cells and, if the two are fabricated from the same resistivity wafer and the same thickness, the response to the long wavelength part of the sun's spectrum will be the same.

There is enough additional power in the short wavelength part of the radiation output of the sun to warrant an interest in investigating the possibility of obtaining a more efficient solar cell with the use of the induced junction. This report considers experiments performed to investigate this possibility.

The amount of additional power that might be available at the shorter wavelengths can be considered by observing the power spectrum from the sun shown in Fig. 4a. Conventional solar cells convert very little of the shorter wavelengths to useful power. Figure 4b shows the spectral response of a conventional cell. The poor response at the shorter wavelengths is due to the fact that these wavelengths create hole-electron pairs at the surface of the cell and must diffuse to the junction to be

collected. Most of them are lost by recombination while travelling to the junction and therefore contribute nothing to the output current.

The inversion layer solar cell differs in several ways from the conventional cell with respect to the collection of hole-electron pairs created at the surface by photons from the sun in the short wavelength part of the spectrum. Most of the effective part of an inversion region is found within .1 μm of the surface and therefore represents a very shallow junction so carriers generated at the surface can be collected before recombination. Because an inversion region is formed by charges outside the surface, a high electric field exists at the surface and extends into the silicon. This field tends to aid the carrier drift to the junction and therefore shorten the time for collection. Thus, most of the holes and electrons created at the surface should be collected. If we assume that all of them are collected in the shorter wavelength region, we can add that part of the spectrum to the power converted by the inversion region solar cell.

If this is so, the response vs. spectrum curve (for equal energy input) might look like the dotted portion of Fig. 4b, where an increase in response in the shorter wavelengths as compared with the response of the conventional cell is evident. (These are not data points but an estimation of the response.) The output of both types when exposed to the energy from the sun is shown in Fig. 5. The dotted curve represents the inversion layer cell and the solid curve the conventional cell. The increase in power output for this estimated determination is roughly 10%. Thus, qualitatively, it can be seen that a greater response of the cell in the shorter wavelengths will yield a greater overall output power of the cell.

In order to induce an inversion layer in a semiconductor surface, a sheet of positive charge must be formed near the surface but isolated from it.

This can be accomplished in several ways. An obvious way is by creating a capacitor on the surface with the semiconductor as the bottom electrode. The insulator must be transparent and the top electrode must be somewhat conductive and also transparent.

Silicon oxide (quartz) is transparent over the spectrum of the sun and can be grown easily on the surface of a silicon wafer by thermal oxidation. Other insulators and other methods can be used to form a dielectric on the surface, but thermally grown SiO_2 will be used in the experiments described here.

Transparent conductors exist, but they have low conductivity. Since the transparent electrode is not in the power circuit of the cell, it is not necessary that this electrode have a very low resistance. A material such as tin oxide will suffice.

A positive bias applied to the transparent electrode with respect to the p semiconducting wafer of sufficient magnitude will cause an inversion layer to grow at the surface. This is one way of obtaining an induced junction and was used in fabricating cells.

Another method of obtaining positive charges above the surface is to supply ions to the SiO_2 layer on the silicon surface, either as it is growing or forcing it through the oxide surface after an oxide layer has been grown. No transparent electrode is necessary because the ions will be the source of positive charge.

Mixing a vapor strongly contaminated with a sodium compound with the oxidizing vapors such as oxygen and water vapor used to grow SiO_2 on silicon will produce an oxide rich in Na atoms and some will be ionized. Other substances can be used but Na was employed in the experiments reported here. This is another way of producing an induced junction and is part of this report.

Yet another way of obtaining a charged layer is to treat the silicon surface such that a large density of donor surface states are created. The

surface represents a drastic change to the ordered crystal structure inside the bulk material and states with energies within the forbidden gap are possible if the interaction with the outside atoms and the silicon surface presents the proper properties. If these states yield an electron to the silicon bulk at the surface, a positive charge is left at the surface, the electron is trapped at the surface, and an inversion layer is formed.

Experiments on cells fabricated to bring out this means of creating an inversion region are part of this report.

A theoretical analysis of the induced junction as a solar cell will be reported. Fundamental equations normally applied to p-n junctions will be used. The boundary conditions and detailed equations peculiar to the induced junction will be applied to the fundamental equations to yield results compatible with the experimental findings. Since the primary use of the solar cell is to extract power from the radiation of the sun, the internal power losses must be kept to a minimum. An important loss of internal power occurs across the internal resistance of the cell. The resistance of the contact between the silicon surface and the metal contacts is an important part of the internal resistance and must be kept as low as possible. Sintered aluminum contacts do not meet the necessary conditions for these contacts, but Ti-Ag contacts or Ti-Pd-Ag contacts do. An attempt to fabricate inversion layer cells with Ti-Ag contacts was made. The problems associated with fabricating the Ti-Ag contact for the inversion layer cell will be presented and discussed.

Experimental results of exposing these cells to various parts of the spectrum of the sun are presented and conclusions drawn that support the claim that the inversion layer cell is more sensitive in the sun's shorter wavelengths than the conventional cell.

II. TRANSPARENT ELECTRODE CELL

A drawing of the transparent electrode cell is found in Fig. 6. The positive layer is formed by applying a bias between a transparent conducting film and the silicon wafer. The conducting film and the surface of the silicon are separated by a layer of oxide thermally grown on the silicon surface.

In order to fabricate a transparent electrode cell, a method of depositing a transparent conductor had to be developed.

A. Transparent Electrode

Not many transparent substances that afford electrical conduction exist. Tin oxide is one such such substance. It can be deposited as a thin film by passing fuming stannic chloride across a hot substrate in the presence of oxygen. Nitrogen is allowed to flow through a beaker containing the stannic chloride and oxygen is allowed to pass through a water bubbler before both are mixed and channelled to flow down the reaction tube. The center of the furnace tube is maintained at a temperature of 530°C. The wafer to be coated is inserted into the tube on a quartz carrier and positioned in the center where the reaction takes place. A diagram of the apparatus is shown in Fig. 7.

Since there is interest in the shorter wavelength sensitivity of the inversion layer solar cell, there should be interest in the transmission of the tin oxide in this region as well as the longer wavelengths. C. W. Morrison in his article in Applied Optics (Vol. 6, No. 3, Mar. 67, p. 573) presents a curve of transmission vs. wavelength for a deposited film of SnO_2. This curve is reproduced in Fig. 8. It is obvious that although there is some attenuation, the response of the cell will not be greatly affected in the short wavelength region.

To ascertain experimentally what the attenuation might be, several slides were coated with a film of SnO_2 and the film etched from half of each slide. Tungsten light was used to illuminate a conventional solar cell through the side of the glass slide with the tin oxide coating and then the side free of the oxide. Short circuit current ratios of .8 - .9 were obtained. Thus, the light attenuation of the thin layer of tin oxide is not serious.

Two solutions are used to etch the transparent conductor. One is an active HCl etch and the other is an HF solution. The HCl is made active by adding zinc to the 1:1 H_2O - HCl solution. The etching takes place while the zinc is reacting with the HCl. This etch is selective so only the SnO_2 is removed leaving the Si or SiO_2 untouched beneath it.

The HF etch is a 6:1 solution. This will also etch SiO_2 and is, therefore, useful when both layers need to be etched together. Both of these etches are compatible with photoresist masking.

B. Transparent Electrode Cell

Transparent electrode inversion layer solar cells were fabricated using the standard processing techniques of the Solid State Engineering Laboratory at The University of Arizona. An outline of this process is found in Appendix I.

Several cells were fabricated with a contact pattern similar to the one used for the conventional cell. Some of these large cells suffered from pin holes that cause shorts and leakage from the transparent electrode to other parts of the cell. Any hole in the oxide can expose the transparent electrode to other parts of the cell. Any hole in the oxide can expose the transparent electrode to the silicon surface. Since the density of

pin holes is not large, smaller cell sizes would increase the chance of obtaining a "good" cell. Information gained from a smaller cell would be just as valuable as a large 2x2 cm cell, so masks were made to reduce the size of each cell from 2x2 cm to .5 x .5 cm. This allows a matrix of 4x4 cells to be fabricated simultaneously on a 2x2 cm wafer. Thus, from the sixteen areas some will be pin hole free and therefore subject to close examination.

Since the area of each cell is small, there is no need for a multiple finger contact pattern. One contact area in the center would suffice. A more useful structure can be made, however, by providing two contact stripes so measurements can be made between them. This arrangement is particularly useful in the contaminated oxide and the surface state cells. The mechanism that creates the inversion regions is effective only in the area between the two stripes. Therefore, a conductance measurement between the two stripes will give an indication of the magnitude of the inversion layer between them. Metallic contact to the top of the silicon is made by an evaporated layer of metal (Al) etched into a grid pattern. The space openings are .4 cm x .4 cm. Within each opening are two stripes of metal separated by .25 cm. An n type diffusion exists under each metallic stripe, in the p type wafer creating two p-n junctions, .35 cm long, .075 cm wide and separated by .25 cm. A .25 cm and .35 cm layer of silicon dioxide topped by a transparent conducting layer of tin oxide is formed on top of the silicon between the two stripes and slightly overlapping each stripe. This configuration is seen in Fig. 9. A cross section of the device is shown in Fig. 10.

When a positive bias is placed between the transparent electrode and the wafer, negative charges are attracted to the top of the silicon between the two n diffusions. Thus, the p type wafer at the surface is converted to n type. The two n diffused stripes are thus connected together by this n layer affording conduction between them. The conductance will depend on the magnitude of the positive bias to the electrode. If a charge already exists on the silicon surface due to filled surface states or contamination, conduction will take place at zero bias. This zero bias conductance can be reduced by applying a negative bias to the transparent electrode, causing the negative charges to leave the surface and convert it back to p type. Once the semiconductor between the two n diffusions is p type, at least one reverse biased junction appears in the current path between the n diffused areas. This limits the current to the reversed bias saturation current I_o.

Thus, a plot of I vs. bias to the transparent electrode will range from I_o to comparatively large values of current. If I is forced through the circuit with a small constant potential (in this case, .1v), then I will be directly proportional to the conductance of the device.

Such a plot for one of the small cells is found in Fig. 11. Measurements were made in the dark to eliminate any photo voltage that might occur and upset the results. From examination of the plot it can be seen that there is an inversion layer at zero bias occurring near .01 ma. This can be attributed to either a trapped surface charge or an ionic charge in the oxide or some of both. Saturation in this plot occurs at near -20V and levels off at 1 μa. Since the area of the reversed biased n diffusion is .3 cm^2, the saturation current is 3.3×10^{-6} A/cm^2. From -20V bias the

curve rises at first in a linear fashion and then bends over as higher bias potentials are applied. Since the current is a direct function of the electron concentration n, and n is a direct function of the applied potential, we would expect the current to be a linear function of the applied bias. The mobility changes, however, causing the nonlinearity.

The thickness of the silicon oxide between the silicon surface and the tin oxide is 6000 Å in this sample. The electrical breakdown potential of 6000 Å on SiO_2 is 360V. Cells similar to the one reported above broke down at 200 volts so measurements were limited to a maximum applied bias of 150V.

The plot in Fig. 11 illustrates the growth of an inversion region and will give us some indication of the concentration of carriers at the surface.

Now the conductance G is equal to

$$G = \sigma \frac{wt}{\ell}$$

but

$$\sigma = qn\mu$$

so

$$n = \frac{G\ell}{q\ wt\ \mu}$$

G at 50V bias = .32 mili mhos

ℓ = .25 cm, w = .35 cm

$\mu = .7 \times 10^3$ $cm^2/Vsec$

and assuming an inversion layer thickness of .1μ, we obtain

$$n = 1.9 \times 10^{17} \text{ carriers/cm}^3.$$

This same parameter can be estimated by considering the capacitive action between electrode and silicon. The capacity between the two can be found by

$$C = \frac{\varepsilon A}{S}$$

A is area of electrode

S is thickness of SiO_2

but

$$Q = CV = \frac{\varepsilon AV}{S}$$

so

$$\frac{Q}{A} = \frac{\varepsilon V}{S}$$

but

$$qnt = \frac{Q}{A}$$

so

$$n = \frac{\varepsilon V}{qtS}$$

where

$\varepsilon = 3.5 \times 10^{-13}$ farad/cm

$V = 50$ volts

$t = .1 \times 10^{-4}$ cm

$S = 6000$ Å

thus, $n = 1.8 \times 10^{17}/\text{cm}^3$, in good agreement with the value of n above.

These are simplified determinations of n because other factors such as the nonlinearity of G vs. bias and the surface charge on the silicon were left out; nevertheless, it does show compatibility between the two methods and gives some confidence that the strength of the inversion layer can be determined by a conductance measurement.

This will be important when we try to determine the strength of the inversion layer when no transparent electrode exists such as in the contaminated oxide cell or the surface state cell.

From the data of conductance vs. bias between the two stripes, a determination of the strength of the inversion layer for the contaminated oxide layer can be obtained. This is accomplished by making a conductance measurement between the two n diffusions and relating this to the bias required to obtain the same conductance.

A schematic of the arrangement of equipment used to make these measurements is found in Fig. 12. The p wafer was connected to the n diffusion on the negative side of the .1 volts so the other pn junction would be reverse biased.

A curve of short circuit current vs. bias on the transparent electrode was made on the cell from series 6 No. 1 wafer mentioned above. The plot for this cell is found in Fig. 13.

Another significant fact to be gained from Fig. 13 is the increase in cell response as a bias is applied. A ratio of $\frac{2.8}{1.2} = 2.3$ is obtained from +150 volts to -50 volts. The curve bends over into a saturation condition as we would expect. The conductance curves do not saturate, however, as shown in Fig. 11. This can be explained because as shown by the

equations derived above for n and G that G is a linear function of n and n is a function of the applied bias V.

Knife Edge Experiment

Another cell on wafer #1, series 6, was chosen to be used to measure a number of interesting things about the inversion cell. A plot of conductance between the n diffusion regions vs. transparent electrode bias for this cell is found in Fig. 14 for a FBE light intensity of 140 mw/cm^2. The plot is similar to the ones on the same wafer.

A new set of data was taken on this cell that was not taken on the others that gives further insight into the effectiveness of the inversion layer as a photon produced charge collector.

Provision was made for a semi-infinite plane with a knife edge to be inserted between the light source and the solar cell surface. The plane was very close to the cell surface so the radiation could be blocked off from a portion of the cell leaving the rest of the cell illuminated. The plane was mounted on a carrier that could be precisely positioned with a micrometer head. Thus, the edge of the plane could be accurately positioned at any point over the cell with respect to an edge of the cell area. The response of the cell as portions of light are prevented from illuminating the cell will indicate how far from the diffusion areas the cell is sensitive to the collection of hole electron pairs generated by photons.

Figure 15 shows the results of cell response (I_{sc}) vs. distance of the knife edge from the edge of the cell area for various values of transparent electrode bias. The edge of the cell area is the edge of the metal grid structure used to contain the p wafer that separates each cell area. The data to plot Fig. 15 was taken by drawing current from only one of the n

diffusion areas, the one farthest from the cell edge at 0 inches. The dark bars at the bottom show the n diffusion areas and the dotted lines are the cell edge areas. An outstanding feature of this family of curves is the extension of the sensitive area as the inversion region grows with bias. If the 90% points of each curve is taken, shown by the arrows, it can be seen that as the inversion region becomes stronger, the sensitive area becomes larger and thus will accept more of the charges created by photons. Therefore, the response of the cell becomes greater and the power output more. At -10V bias the 90% point is .02 inches from the near edge of the diffusion region used to extract power, whereas at +80V bias the 90% point is .03 inches from the edge of the diffusion region. At -20V bias the charges diffuse to the depletion area of the diffused p-n junction and are collected there but when an inversion region exists in this region, the charges can be separated by the induced p-n junction at the surface increasing the probability of a collection before recombination. At distances greater than .03 inches from the diffusion area or distances less than .078 inches from the edge of the cell area no increase of response is observed as light impinges on this area because the hole-electron pairs created there recombine before reaching the n diffusion area even though collected by the inversion layer. The linear response from the near edge of the diffusion region as the light is eliminated over the diffused area is due to the fuzzy edge of light on the cell due to the diffuse nature of the FBE light source and the distance the knife edge had to be above the cell in order to clear probes to the conducting areas.

Nevertheless this region is not affected by the bias and, therefore, not affected by the inversion layer. The diffusion length is about .015 inches for minority carriers in the p wafer.

An interesting parallel to the analysis of Fig. 15 is found in Fig. 16. Here the same type of curves were made but both n diffusion regions were connected together. For a -20V bias the photons at the middle of the cell generate charges that do not reach either depletion region and thus a flat portion occurs.

Figure 17 shows a similar plot of knife edge vs. I_{sc} response for a mercury vapor light source. This light source is a point source and therefore much less diffuse than the FBE lamp and the shadow edge is much sharper. Therefore, we do not see the characteristic slope at the end of the curve as for the FBE lamp. This curve acts as would be expected; that is, the curve flattens out as it passes over the aluminum on the active diffusion area and sharply dips at the end as the sharp shadow passed over the exposed area between the n diffusion and the edge of the cell or aluminum matrix. A marked difference in the extent of influence of the light when the inversion layer is present than when it is not, is brought out by comparing the 80V and -20V curves in this figure. The ultraviolet rich source will create holes and electrons near the surface where they can be separated by the strong field there before recombining.

Figure 18 shows this same cell in response to the UV source. Only one contact was used. This source is a diffuse source so we have a fuzzy shadow as in the FBE lamp and a slope exists at both ends for the 0V to 80V bias. The slope exists at the left end because the collection of carriers for these wavelengths extends across the cell and the aluminum over the diffusion area blocks out the light. The -20V bias curve collects carriers from a greater distance than for white light but not as much as when the inversion layer is present.

Thus, it has been demonstrated by this set of experiments that the induced p-n junction and associated electric field does indeed separate the hole-electron pairs created by photon irradiation.

Evidence also points to this cell being extra sensitive to the ultraviolet spectrum. It was also pointed out that the separation of the n diffused areas for optimum collection should be closer than the separation of the n diffusion in the test cells.

I-V Curves

A curve of solar cell current vs. cell output voltage for the transparent electrode cell is found in Fig. 19. Biases of -20, 0, 40 and 80 volts were used. The illumination of the FBE lamp was adjusted for 140 mw/cm^2. The maximum power at a bias of 80V is about .51 milliwatts, at a bias of 40 about .47 milliwatts, at 0V about .4 mw, and at 0 bias about .3 mw. Since the area of the small cell is about .1 cm^2, the efficiency of the cell at 80V bias is

$$\frac{.51}{140 \times .1} = .036 \quad 3.6\% \quad ,$$

and the efficiency of the -20V bias is

$$\frac{.3}{14} = 2.1\% \quad .$$

The short circuit current - open circuit voltage at 80 volts bias product yields an efficiency of

$$\frac{.48 \times 2.3}{14} = .079 = 7.9\% \quad .$$

III. CONTAMINATED OXIDE CELL

A. Contaminated Oxide Growth

In the fabrication of inversion layer solar cells, standard solid state laboratory processing techniques were used whenever possible. However, due to the nature of the contaminants being used (sodium compounds), it was necessary to prepare a special furnace to thermally grow silicon dioxide impregnated with positively charged sodium ions. Oxygen and nitrogen gases were metered and valved so combinations of flowrates of either or both gases could be passed down the quartz tube heated by the furnace to 1050°C. An alternate path for oxygen was provided through a bubbler. If pure water is used in the bubbler, a steam oxide can be grown on a silicon wafer comparatively free of contaminated ions. If a substance rich in ions was dissolved in the water, some of the substance would carry over with the water vapor and contaminate the oxide, thus providing positive charge sources in the oxide. The physical arrangement used to accomplish this oxide growth is shown in Fig. 20.

B. Sodium Compound Contamination

Previous studies made on MOS transistors long ago established the fact that sodium can act as a source for positive charge. Therefore, sodium chloride was selected initially as the source of the contaminating ions. Other sodium compounds such as NaOH, NaBr, and NaI were used in the bubbler in an endeavor to optimize the contamination in relation to cell response (I_{SC}). Experimental data revealed that the best source of positive ions which could be applied as described was NaCl.

The small cell configuration was used to fabricate a number of contaminated oxide solar cells. The oxide over the area between the n-diffusion

stripes was grown with a vapor formed by bubbling oxygen through a NaCl solution at 100°C. Thus, the oxide was interspersed with Na atoms, some of which were positively ionized. This positive charge in the oxide caused electrons to accumulate at the oxide-silicon interface and produce an inversion layer in the semiconductor.

The steps used in processing these solar cells are outlined as follows:

1. SiO_2 was grown on wafers for 50 minutes at 1100°C producing a 6000 Å layer of oxide.
2. The small cell grid pattern was then etched through the oxide using conventional photoresist process.
3. A 15 minute predeposition of n-type dopant (phosphorus) was accomplished using standard procedures.
4. The initial oxide growth was completely removed from the front and back of the wafer.
5. Using the special furnace, a contaminated oxide was grown on the wafer.
6. This layer of oxide was etched with the photoresist process to provide a grid pattern on the diffusion areas, but was smaller than the diffusion areas.
7. Aluminum was vacuum deposited on front of wafer.
8. Aluminum was then etched into the proper grid pattern.

B. Cell Characteristic Measurements

For all series of wafers processed, 10 ohm-cm, 2x2 cm, p-type wafers were used. Each series consisted for four wafers, each with sixteen small solar cells. Each of the small cells underwent a series of measurements

to determine the cell characteristics. Measurement of the integral and spectral characteristics of the cells was accomplished to obtain the following:

1. Cell response to tungsten illumination. The illumination was adjusted using a JPL calibrated secondary standard silicon solar cell. The current-voltage characteristics under illumination were measured and the short-circuit current, open-circuit voltage, and maximum power points were obtained.
2. Cell response to sun-simulated illumination. Since the inversion layer solar cell theoretically had a greater response in ultraviolet light than conventional p-n junction solar cells, investigation was conducted by illuminating with an ultraviolet rich source with a spectrum beyond that obtainable with tungsten sources. Measurements as in (1) above were made. The illumination was again adjusted using the calibrated secondary standard silicon solar cell.

D. Contaminated Oxide Thickness and I_{SC}

Several wafers were processed with different thicknesses of contaminated oxide, thinking that if the distribution of Na atoms is uniform in the oxide, the total charge density would be a function of the oxide thickness. Therefore, the inversion layer strength should increase with oxide thickness and consequently, so should the response of the cell. Oxide thicknesses were varied by subjecting each wafer to the same vapor flow but for different lengths of time in the furnace. The short-circuit current was then measured for each of the sixteen small cells on each wafer. These values were then added and averaged for each separate wafer to obtain a

wafer average value for I_{SC}. The results of this experiment are shown by the two curves in Fig. 21.

A definite increase in average I_{SC} is noted in the thicker oxide up to an oxide thickness of approximately 5000 Å, at which point the I_{SC} values approach a maximum. The observed leveling is the result of two factors. First, the thicker oxides produce higher inversion densities, thereby causing a decrease in carrier mobilities and causing a nonlinear relation of hole-electron collection with inversion layer strength.

Secondly, there exists the probability that, for the thicker oxides, the positive ions induce negative charges at the outside surface of the oxide rather than at the oxide-silicon interface. Thus, not all of the ions in the oxide are effective and a linear growth of inversion layer strength should not be expected for a linear growth of oxide even though the concentration of ionic contaminants is uniformly distributed throughout the oxide. In fact, if the oxide is thick enough, none of the ions at the top surface will induce electrons at the silicon surface, but will trap a negative charge on the outside surface of the oxide.

If the curves are extended to zero oxide thickness at the lower ends, a value of about 1 ma I_{SC} was noted. This is compatible with the I_{SC} of a bare p-n junction under an intensity of 140 mw/cm^2. The optimum oxide thickness was determined to be within the 3500-4000 Å range. This is the area of merger of two curves and is the oxide thickness selected for experiments designed to optimize contamination solution concentration and selection of the best sodium compound to provide positive ions.

An unusual aspect of this experiment is the fact that two curves evolved from measuring the I_{sc} on each of the 16 small cells and averaging to obtain an average I_{sc} for a number of wafers whose only difference is the

oxide thickness for the entire wafer and yet have the results from each wafer plot on either of the two curves in Fig. 21 rather than on just one curve. It is apparent that different conditions at the surface or in the oxide can cause different inversion intensities. Why there is this difference has not been determined, but variations can occur as a result of processing especially when surface phenomena is an important factor.

To further show that the oxide, in fact, does hold an influence over the output of the cell, a wafer with an oxide thickness of 3600 Å was subjected to a number of etches that removed the contaminated oxide in incremental steps. The wafer chosen had an output of 2.1 ma I_{sc} for an illumination of 140 mw/cm^2 from a tungsten lamp. The incremental steps yielded oxide thicknesses of 2900, 2100, 1600, 700, 200, and 0 Angstroms. The average output of the cells on the wafer was measured at each step. The results of this etch and measurement process are shown in Fig. 22. This process was then repeated with a wafer having a 7100 Å oxide layer and an I_{sc} output of 2.34 ma after the initial processing. The results of that process are shown in Fig. 23.

It can be seen from Figs. 21, 22, and 23 that ionic contamination can create an inversion layer of sufficient strength to affect the power output of the cell. Also, the strength of the inversion layer is a function of oxide thickness due to the uniform distribution of positive ions in the oxide. The existence of a uniform distribution was verified by the plots in Figs. 22 and 23.

E. Inversion Layer Sensitivity

In an attempt to determine the sensitivity of the inversion layer, one of the small cells and the conventional p-n junction solar cell were both exposed to a light source strong in ultraviolet. The small inversion cell selected for this experiment displayed an I_{sc} of 3.0 ma when subjected

to tungsten illumination of sunlight intensity. When exposed to an ultraviolet source, an I_{SC} of 63 μa was recorded. An indication of the relative response of the two different cells was obtained by exposing the conventional cell to the same tungsten and ultraviolet source as that used for the inversion layer cell. The results are as follows:

	Tungsten Source	Ultraviolet Source
Conventional Cell (I_{SC})	133 ma	.22 ma
Inversion Layer cell (I_{SC})	3.0 ma	.063 ma

The ratio of the short circuit currents for the two cells for the tungsten source is 133/3.0 or 44. That is, the conventional cell generates 44 times as much I_{SC} as the inversion layer cell. However, from the U.V. source the ratio is .22/.063 or 3.5. So the conventional cell does not generate nearly as much in proportion to the inversion layer cell. Therefore, the power output for this part of the spectrum should be much greater for the inversion cell. The area of one of the small inversion cells is approximately 1/40 the area of the conventional 2x2 cm cell. If we use this factor, a 2x2 inversion cell would produce 3.0 ma x 40 or 120 ma compared to the 133 ma for the conventional cell if flooded with 140 mw/cm^2 of incandescent light. But if exposed to U.V. light only, the 2x2 cm inversion cell would produce .063 ma x 40 or 2.52 ma compared with .22 ma for the conventional cell. This result is compatible with the claim that the inversion cell should be more sensitive in the U.V. because the hole-electron pairs are created at the surface in a strong electric field and this field separates the carriers quickly before recombination can occur.

A study was made of the U.V. response of the inversion cell as a function of oxide thickness. The previously described incremental etching procedure was used to measure U.V. I_{SC} at various contaminated oxide thicknesses. These measurements revealed that U.V. response did not vary with oxide thickness but that U.V. response was relatively constant as long as any oxide at all existed on the solar cell. Therefore, even the weakest intensity electric field created by the inversion layer was adequate to collect the hole-electron pairs before they could recombine.

Another attempt to observe the affect of a change in spectrum was tried by using still another different light source. A mercury vapor source rich in ultraviolet, but containing a spectrum in the visible also, was used on the two cells for comparison. The same analysis was made as before by looking at the ratio of I_{SC} for the conventional cell with respect to the inversion cell.

	Tungsten Source	Hg Source
Conventional Cell (I_{SC})	133 ma	17 ma
Inversion Layer Cell (I_{SC})	3.0 ma	.54 ma

The ratios are:

$$\frac{\text{Conv. cell}}{\text{Inv. cell}} \text{ (tungsten)} = \frac{133}{3.0} = 44$$

$$\frac{\text{Conv. cell}}{\text{Inv. cell}} \text{ (Hg)} = \frac{17}{.54} = 30$$

Again, the evidence reveals that an ultraviolet rich source will decrease the ratio between the conventional cell I_{SC} and the inversion cell I_{SC}, thereby establishing the inversion layer as more efficient in the U.V. region.

F. Knife Edge Measurements

In order to gain further insight into the effectiveness of the inversion layer as a charge collector, provisions were made for a semi-infinite plane with a knife edge to be inserted between the light source and the solar cell surface at a point near the surface. The response of the cell as portions of light are prevented from illuminating the cell will indicate how far from the diffusion areas the cell is sensitive to the collection of hole-electron pairs generated by photons. Figure 24 shows the results of cell response (I_{SC}) vs. distance of the knife edge from the edge of the cell area for various contaminated oxide thicknesses. The edge of the cell area is the edge of the metal grid structure used to separate each cell area. The data to plot Fig. 24 was taken by drawing current from only one of the n-diffusion areas, the one farthest from the cell edge at 0 inches. The dark bars at the bottom show the n-diffusion areas. Points at which I_{SC} is maximum and zero are the cell area edges.

An outstanding feature of the family of curves of Fig. 24 is the extension of the sensitive area as the inversion region grows with oxide thickness. If the 90% point of each curve is taken (shown by the arrows), it can be seen that as the inversion region becomes stronger, the sensitive area becomes larger and thus will accept more of the charges created by photons. Therefore, the response of the cell becomes greater and the power output more. At distances greater than .03 inches from the diffusion area or distances less than .07 inches from the edge of the cell area, no increase in response is observed as light impinges on this area. This occurs because the hole-electron pairs created there recombine before reaching the n-diffusion area even though they are collected by the inversion layer. This

somewhat indicates the strength of the electric field created by the inversion layer if one compares the normal diffusion length of minority carriers in the p-type wafer (.015 inches) to the collection distance (.03 inches) from the n-diffusion areas.

An interesting parallel to the above analysis was made by connecting both n-diffusion regions into the test circuit. These curves are shown in Fig. 25. For cells with oxide thicknesses of 0-2800 Å, the photons at the middle of the cell generate charges that do not reach either depletion region and thus a flat portion occurs. For the cell with 700 Å of oxide a flat portion should occur but should be shorter than the 1250 Å curve and shorter at both ends. For the cell with 3600 Å of oxide there is response (I_{SC}) across the entire length of the cell as one would expect because of the presence of the inversion layer. At about .06 inches a lump can be noted. This is due to the bending of the curve from the collection of carriers by the left n-diffusion and the influence of the collection of carriers by the right n-diffusion. The curve could approximate a straight line by placing the two diffusion areas closer together. Placing them very close would cause the diffusion length to overlap and straighten the 0-2800 Å of oxide curves.

Thus, it was demonstrated by this set of experiments that the induced p-n junction and associated electric field does indeed separate the hole-electron pairs created by photon irradiation.

Evidence also points to this cell being extra sensitive to the ultraviolet spectrum. It was also pointed out that the separation of the n-diffused areas for optimum collection should be closer than the separation of the n-diffusions of the test cells.

IV. SURFACE STATE SOLAR CELL

Different methods of treating the surface of a silicon wafer to create occupied surface states during the fabrication of inversion layer solar cells were tried. Small area solar cell masks described above were used to fabricate cells with different processing procedures. Four 2 cm x 2 cm wafers with the small cell patterns were processed in four different ways.

A. Fabrication

The first wafer was processed in the following way after the n diffusion:

1. The final oxide was grown for 12 minutes using steam and oxygen.
2. The wafer was pulled slowly from the furnace with steam and oxygen on.
3. Holes in the oxide were etched for aluminization.
4. The wafer was aluminized and etched.
5. The wafer was sintered for 4 minutes at 480°C.

The average short circuit current over the 12 cells on this wafer was 2.08 ma for an illumination of 140 mw/cm^2 from a FBE incandescent light source. Variation of I_{SC} response from cell to cell over the wafer ranged from 1.9 ma to 2.1 ma. 2.08 can be compared to the transparent electrode cell of the same configuration where a bias changed the cell from 1.2 ma to 2.8 ma (+160V). Thus, there is an inversion region created by mechanisms at the surface or in the oxide or both.

The second wafer was processed as the first wafer except the aluminum in Step 4 was sintered before it was etched. Thus, the aluminum over the oxide over the sensitive portion of the cell is allowed to interact

with the top surface and reduce the surface states at the $Si-SiO_2$ interface. This annealing effect is probably due to the interaction of the aluminum with a slight trace of water at the top surface. This interaction produces hydrogen and hydrogen diffuses rapidly through the oxide at the sintering temperatures and partially pacifies the surface states at the interface. Thus, the response of the cells on wafer #2 should be less than the response on wafer #1. Such is the case because the average I_{SC} for the cells on wafer #2 is 1.58 ma with a variation across the wafer of 1.5-1.7 ma. This is a significant change compared to wafer #1 and illustrates how a change in processing can effect a change in the strength of the inversion layer.

Another wafer was processed differently than wafer #1 or #2. Whereas in the first two wafers, both steam and oxygen were left on in steps 2 and 3, only oxygen was left on in fabricating wafer #3.

Steps 1, 4, 5 and 6 are the same as wafer #1. The schedule is like this:

1. During final oxidation 7 minutes of oxide was grown using steam and oxygen.
2. The steam was then turned off and the wafer was left in the furnace for 5 minutes with dry oxygen on.
3. Wafer was then pulled out slowly with dry oxygen on.
4. Pre-ohmic holes were cut in oxide.
5. Wafer was aluminized and etched.
6. Wafer was sintered for 4 minutes at 480°C.

B. Results

The average short circuit current over the twelve cells is 1.66 ma with a spread of 1.2-2.0 ma. The average is significantly less than wafer #1 but the spread is much larger than wafer #1. Thus, there is a difference in I_{sc} between wafer #1 and wafer #3 which indicates that whether steam is present or not, as the wafer cools, does affect the surface states and thereby the magnitude of the inversion region.

Another variation in processing was tried in fabricating wafer #4. The procedure is essentially the same as wafer #3 but nitrogen was used in Step 2 and 3 instead of oxygen. Steps 1, 4, 5 and 6 are the same as wafer #1 and #3. The average I_{sc} for this group of cells was 1.78 ma with a spread of 1.4-2.0 ma.

A summary of the results of this experiment is found below.

	Average I_{sc}	Spread
Both steam and O_2 left on	2.08 ma	1.9-2.1 ma
Aluminum sintered before etch	1.58 ma	1.5-1.7 ma
Only O_2 left on	1.66 ma	1.2-2.0 ma
Only N_2 left on	1.78 ma	1.4-2.0 ma

The results of this experiment show a change in inversion layer is possible with a change in processing. This can be attributed to surface state phenomena since the other source of induction, contamination, should be a minimum.

Another wafer was processed to investigate surface state creation of inversion layers. The following procedure was used to process the wafer:

1. Normal process through diffusion step.

2. All oxide was stripped from wafer.
3. 4500 Å of steam oxide was grown.
4. Wafer was slowly pulled from furnace with steam on.
5. Pre-ohmic holes were cut.
6. Wafer was aluminized and sintered for 4 minutes at 480°C.

All sixteen cells on the wafer responded to illumination from the FBE incandescent lamp. Short circuit current ranging from 1.6 to 2.8 ma were measured. The average over the wafer was 2.14 ma. The individual currents were (all in ma):

2.1, 1.9, 1.6, 1.9, 2.0, 2.1, 2.1, 2.0, 2.1, 2.1, 2.1,

2.0, 2.8, 2.6, 2.5, 2.3.

The response of the last four cells is higher than the average and they were all located along one edge of the cell, showing that a high response can be achieved by proper treatment of the silicon surface during fabrication.

V. THEORETICAL ANALYSIS

The approach to the determination of the currents and voltages expected with this cell is similar to the approach taken to analyze the conventional diode with a graded junction. The equation

$$J = J_n + J_p = qD_n \frac{\partial n}{\partial x} + qn\mu_n E - qD_p \frac{\partial p}{\partial x} + qp\mu_p E$$

is used to obtain the current density. As a first approximation, the E field is neglected and the diffusion terms retained. Since the p side is similar to a conventional diode, it will be handled similarly.

The n side, however, is due to the distribution of inversion layer electrons and involves equations derived from consideration of phonomena at the surface.

If we combine Poisson's equation

$$\frac{\partial^2 \psi}{\partial x^2} = - \frac{\rho(x)}{\varepsilon_s}$$

with the charge density inside the semiconductor

$$\rho(x) = q(N_D - N_A + P_p - n_p)$$

and considering

$$P_p - n_p = P_{po} e^{-\beta\psi} - n_{po} e^{\beta\psi}$$

then

$$\frac{\partial \psi}{\partial x} = - \frac{2}{\beta L_D} \left[(e^{-\beta\psi} + \beta\psi - 1) + \frac{n_{po}}{P_{po}} (e^{\beta\psi} - \beta\psi - 1) \right]^{1/2}$$

where

$$\beta = \frac{q}{kT} \quad ,$$

when we are interested in the strong inversion region where $\psi\beta >> 1$ or

$$e^{\beta\psi} >> \beta\psi >> 1 \quad .$$

The above equation reduces to:

$$\frac{\partial\psi}{\partial x} = - \frac{2}{BL_D} \sqrt{\frac{n_{po}}{p_{po}}} \; e^{\beta\psi/2} \; .$$

Integrating over the limits from the surface where the surface band bending potential is ψ_s at x = o to a point within the surface at x, we get:

$$x = L_D \sqrt{\frac{p_{po}}{n_{po}}} \left[e^{-\beta\psi/2} - e^{-\beta\psi_s/2} \right]$$

but

$$n(x) = n_{po} \; e^{-\beta\psi}$$

and finally

$$n(x) = \frac{n_{po}}{\left[\frac{x}{L_D} \sqrt{\frac{n_{po}}{p_{po}}} + e^{-\beta\psi_s/2} \right]^2}$$

In order, though, to obtain a reasonable result for the current flowing across the depletion region, the gradients of electrons and holes at the depletion region have to be known. Mathematical expressions exist that can give these relationships but boundary conditions must be determined from judgments made about the onset of strong inversion and weak inversion. Strong inversion occurs at the points where the Fermi level, with respect to the mid-band energy, is equal but opposite to the Fermi level in the

bulk. This can be illustrated in Fig. 26. This figure represents the forbidden band of a semiconductor with the bottom of the conduction band on top and the top of the valence band on the bottom. E_i is in the middle of the forbidden band. E_F is the Fermi level. An indicator of whether a semiconductor is n or p type is whether the Fermi level is above (n) or below (p) E_i. A measure of the magnitude of n or p is the position of the Fermi level with respect to either the valence band for p type or the conduction band for n type. The closer to either band the more heavy is the carrier concentration. Thus, when the bands bend and E_i crosses over the E_F, a semiconductor near the surface can change from p to n as shown. Thus, a p-n junction is formed at the surface.

The shape of the band as it bends toward the surface can be obtained from a theoretical analysis of the inversion process. A plot of ψ vs. x is shown in Fig. 27. This is the shape of the bands near the surface. Of course, the shape depends on the magnitude of the final deviation at the surface ψ_s. Figure 27 is the plot for a ψ_s of .65 volts, Fig. 28 for a ψ_s of .70 volts and Fig. 29 for a ψ_s of .75 volts. These surface potentials correspond to a surface concentration of electrons of 10^{16}, $5x10^{16}$ and 10^{17} respectively, assuming room temperature and wafers of 10 ohm-cm p type. The equation integrated to obtain these three plots is:

$$\frac{\partial\psi}{\partial x} = \frac{2}{BL_D}\left[e^{-\beta\psi} + \beta\psi - 1 + \frac{n_{po}}{p_{po}}(e^{\beta\psi} - \beta\psi - 1)\right]^{1/2}$$

(See Physics of Semiconductor Devices, Sze, Wiley, p. 431.)

where

$$\beta = \frac{q}{kT}$$

L_D = diffusion length

n_{po} = electron concentration in the bulk

p_{po} = hole concentration in the bulk

The onset of strong inversion is at the point where $\psi = .6$. From the plot for $\psi_s = .75$ this corresponds to a point .06 μmeters into the silicon surface and for .65 volts ψ_s about .03 μmeters.

The onset of inversion occurs where $\psi = \psi_\beta = .3$ volts. For $\psi_s = .65$ inversion starts at 3 μmeters and when $\psi_s = .75$ inversion starts about the same. Thus, the boundary points can be determined from these plots.

The surface potential ψ_s was obtained by applying an external potential to the transparent electrode. A plot of the external bias to the transparent electrode vs. the ψ_s it creates is found in Fig. 30. The equation used for this plot is:

$$V_{applied} = \psi_s + \frac{qD_s}{\epsilon} \left[u_d + u_w\right]$$

where

$$u_w = p_{po} \left[\left(\frac{2\epsilon\psi_s}{p_{po}} \right)^{1/2} - d \right]$$

and

$$u_d = L_D\, n_i \left(e^{\beta\psi_s/2} - \frac{1}{\frac{d}{L_D}\sqrt{\frac{n_{po}}{p_{po}}} + e^{\beta\psi_s/2}} \right)$$

d is the inversion thickness

n_i is the intrinsic concentration

Figure 31 is an approximate plot of electron concentration vs. depth into the wafer for two values of surface potential .65 and .75 volts. The two vertical lines represent the value at strong inversion. The left one for the lower .65 volt curve and the right one for the .75 volt curve. The equation used to obtain this plot is: (when $\beta\psi >> 1$)

$$\frac{\partial\psi}{\partial x} = \frac{2}{BL_D} \sqrt{\frac{n_{po}}{p_{po}} e^{\beta\psi}}$$

and $n = n_{po}\, e^{\beta\psi}$.

Simple theory indicates that conductance, G, between the two stripes of the small cell should be a linear function of the bias applied to the transparent electrode of the transparent electrode solar cell. The equation describing this relationship is:

$$G = \frac{\mu w \epsilon V}{\ell s}$$

where μ carrier mobility

w width of cell

ϵ permittivity of dielectric SiO_2

V applied bias to transparent electrode

ℓ length of cell

s thickness of dielectric

Thus, if μ, w, ϵ, ℓ and s are all constants, then G is directly proportional to V and a plot of G vs. V should be a straight line with slope $\frac{\mu w \epsilon}{\ell s}$.

However, a plot of G vs. V for a small cell is not a straight line but bends over for large values of bias. This is illustrated in Fig. 32. Since w, ℓ and s are physical dimensions, they are not likely to change and

changes in ϵ will be negligible, so these influences will not cause the change in slope. However, μ does change as the concentration of electrons changes in the inversion layer.

This change in mobility for a change in electron concentration is well known and is explained in the book, "Semiconductors" by H. Wolf published by Wiley. Page 402 in this book contains curves of μ_{eff} vs. carrier concentration for inversion layers.

To obtain a calculated curve of G vs. applied bias, a computer-aided plot of μ_{eff} vs. surface voltage (ψ_s) was made from the equations found in Wolf:

$$\mu_{eff} = \frac{\mu_B \mu_s}{\mu_B + \mu_s}$$

$$\frac{\mu_s}{\mu_B} = 1 - e^{\alpha_s^2} \text{ efc } (\alpha_s)$$

$$\alpha_s = \frac{1}{E_s \mu_B} \left[\frac{2kT}{m_n}\right]^{1/2}$$

Curves of E_s vs. surface voltage (ψ_s) were computed so a plot of μ_{eff} vs. ψ_s was possible and is found in Fig. 33. A plot of ψ_s vs. applied bias was also available, so a plot of μ_{eff} vs. applied bias is possible. Since μ is directly proportional to G, a plot of μ vs. applied bias could be applied to the experimental curve of G vs. applied bias.

This experimental curve, however, does not meet the origin at 0 bias because of other sources of charge creating the inversion layer beside the applied bias. To bring the two curves together they were both normalized at 100 volts bias and the experimental curve shifted by 17 volts. Fig. 34 shows the results of this comparison. The dotted line is the computer-aided

calculation and the solid line is the experimental curve taken from Fig. 32 A fairly good match is noted. The deviation comes at large values of bias.

Thus the departure from the linearity of G as the inversion layer grows is undoubtedly mainly due to the change of mobility of the electrons as the layer grows. The response of the solar cell is therefore affected by this change in mobility and we should see a "flattening" of the curve for large biases as we do. There are other factors besides the mobility change that flattens the response curve so an exact correlation between the two is not possible.

It has been shown, however, that the change in mobility of the electrons at the surface has a gross effect on the conductivity of the inversion layer and, therefore, a gross effect on the response of the solar cell to illumination.

VI. MEASURING APPARATUS

To enable accurate measurements of current to be made, a temperature controlled cell holder was constructed. The holder was made from a block of aluminum machined to form chambers under the top surface to allow water to circulate in the block. The water is pumped from the tank of a constant temperature bath to the water cooled block. Provision is made for the insertion of the standard solar cell in the circulating path. A thermocouple well was made so a thermocouple could be inserted in the block close to the surface near the cell position. The temperature will be measured by this thermocouple and regulated by adjusting the temperature of the bath water.

Three probes are mounted near the block so an electrical connection can be made to the cell under test. The platform, containing the block and probes, is mounted on an adjustable swivel to allow the cell to be oriented normal to the sun rays. The entire apparatus including the constant temperature bath can be used on a movable cart for easy transportation in and out of the building for a choice of illumination from an inside tungsten source or the outside sun source. The inside tungsten source is a FBE daylight flood light (650W).

Four conventional solar cells were calibrated against the standard cell supplied by JPL. These four cells will be used as substandards to calibrate the inside light source and to determine the sun's intensity when measuring outside.

The standard cell was set in place in the measuring apparatus and one of the substandards set on the aluminum block as mentioned above. The circulating water bath temperature was adjusted to 28°C and a measurement

made on the short circuit current of the standard cell. A value of 40.81 ma was obtained. At 28°C and 140 mw/cm^2 the standard cell will supply a short circuit current of 47.88 ma. Therefore, the sun's intensity at the time of measurement was 119 mw/cm^2. The substandard cells produced short circuit currents of 122.4 ma, 125.5 ma, 122.4 ma and 123.4 ma all at 28°C. The calibration current of these four substandards with respect to an illumination of 140 mw/cm^2 is 143.6 ma, 147.2 ma, 143.6 ma, and 144.8 ma. The substandards were 2x2 cm cells whereas the standard cell was 1x2 cm.

VII. SPECTRAL RESPONSE

Spectral response information on the inversion layer cell is of interest because of the possibility of this cell generating more power in the shorter wavelengths of the sun's spectrum than the conventional p-n solar cell. This possibility arises from the characteristic shallow junction of the inversion layer and the presence of an electric field at the cell surface.

Both of these conditions tend to separate hole-electron pairs created at the silicon surface. To illustrate this, an experiment was performed to obtain a comparison of the response of the transparent electrode cell to the sun with respect to an FBE photoflood lamp. The results show a short circuit current increase of about 10% when illuminated by the sun with respect to the photoflood illumination. This result is shown in Fig. 35.

The two curves in Fig. 35 were plotted from data obtained by illuminating the cell with 120 mw/cm^2, which is the sun's intensity at noon in Tucson. The 120 mw/cm^2 figure was obtained by exposing a conventional cell (calibrated at 133 ma short circuit current for 140 mw/cm^2 illumination) to the sun and getting a short circuit current measurement of 110 ma. This corresponds to an illumination of

$$\frac{110}{133} \times 140 = 120 \text{ mw/cm}^2.$$

The curve labelled "sun illumination" is the curve obtained in the sun as a function of the bias on the transparent electrode.

The intensity of the photoflood light source was set to illuminate the conventional cell so an I_{sc} output of 110 ma was obtained. Data on the

transparent electrode were then obtained at this illumination and is plotted as the lower curve labelled photoflood illumination in Fig. 35.

Thus, the transparent electrode is more sensitive to the radiation from the sun than with radiation from an incandescent source when the two sources are adjusted for equal response to a conventional solar cell.

This phenomena can be explained by considering the difference in spectral distribution between the sun and the photoflood lamp. If the conventional cell is not as sensitive as the inversion layer cell to a part of the spectrum, the shorter wavelengths for instance, but both are equally sensitive to the rest of the spectrum and the two cells are exposed to two different light sources, one containing the short wavelengths and the other deficient in short wavelengths, then the inversion layer cell will show a greater output for the spectrum with the short wavelengths. The reason for this stems from using the conventional cell as a calibrator. The same short circuit current is demanded of both light sources so the illumination in the spectrum that both cells are sensitive to is the same in both but added to this is the part of the spectrum in the short wavelength source that only the inversion layer cell can convert to external current. For the tungsten light source no extra radiation exists that the inversion layer cell is sensitive to that conventional cell is not.

It is interesting to notice that as the inversion layer grows, so does the difference between the response to the two light sources, and where there is no inversion layer (at negative biases) there is no difference between the two sources of illumination. This supports the conjecture that the high field at the surface of the silicon aids the collection of the hole-electron pairs created at the surface by the short wavelength part of the spectrum.

Another evidence that supports the claim that the inversion layer solar cell is more sensitive to the shorter wavelength of the sun's spectrum than the conventional solar cell comes from measurements of cell output made by interposing optical transmission filters between the light source and the cell.

A series of six broadband interference filters was purchased from Baird Atomic Inc. and used to obtain data on the spectral response of the transparent electrode solar cell and the contaminated oxide cell. The five filters have peak wavelengths of 400, 450, 500, 550, 600 and 650 nanometers. The spread at 50% of peak is around 250 nanometers for each filter. Transmission averages 50%.

Light from the sun was used to determine the response of the cells to various parts of the spectrum. Measurements were made on clear days near noon to keep atmospheric absorption to a minimum. The apparatus holding the cell was tilted toward the sun to obtain maximum exposure to the radiation.

A nearly light tight shield was placed around the cell to avoid extraneous light from creating a large background. The radiation impinged on the cell through a hole in the top of the shield. The filters were placed over the hole to obtain the response of the cell to various slices of the spectrum of the light source. An opaque medium was placed over the filter, when in place, to obtain the background response.

Curves of short circuit current vs. wavelength were made for each of the three cells. The curve for the conventional cell is found in Fig. 36. The current measurements in the sun are adjusted to yield values as if 140 mw/cm^2 total radiation was hitting the solar cell. The sharp decrease for

the shorter wavelengths reflects a decrease in the response of the cell plus a decrease in the output of the two sources.

The data was adjusted for each filter according to the amount of radiation allowed through the filter. The factor for each filter was obtained by considering the bandwidth at 50% of peak and the peak transmittance. The reciprocal of the product of these two parameters was used to obtain a weighting factor so somewhat of a comparison could be made between points on the curve.

Figure 37 shows the effect of the sun's radiation on the short circuit current of a contaminated oxide cell. The expected fall off is seen and the difference between the natural and the artificial source is also noted.

Figure 38 shows the curves for a transparent electrode cell for two values of electrode bias. A bias of -20 volts will completely negates any inversion layer and a bias of +50 volts will saturate the inversion layer at these light levels. Therefore, we can observe the effect of the bias on the response at different wavelengths.

The enhancement of the cell as the bias is increased can be measured by comparing the sensitivity at +50 volts to that at -20 volts. This ratio is about 3 for the sun's radiation.

The comparison between these curves as they are displayed on the same axis, as shown in Fig. 39. The data from the conventional cell was multiplied by a factor to make the conventional cell and the transparent electrode cell match at a wavelength of 650 nonometers. The contaminated oxide cell was plotted with no alteration of the data.

The response of the transparent electrode cell and the contaminated oxide cell to the wavelengths of 400 and 450 nanometers upon exposure to the sun is the same. This we would expect because both are inversion layer devices. There is a difference between the two cells for the other wavelengths but since the oxide thickness is different between them the reflection and interference of light will be different also and thus the shape of the curves will not necessarily be the same.

There is a decided difference, though, between the inversion layer cells and the conventional cell. The ratios between values of I_{sc} for the transparent electrode cell and the conventional cell for various wavelengths are found in the following table:

Wavelengths (nanometers)	Ratio
400	4.40
450	1.60
500	1.20
550	1.25
600	1.10
650	1.00

This data establishes that the inversion cell is definitely more sensitive to the shorter wavelengths than a conventional cell. If the shorter wavelengths of 300 and 350 nanometers were explored even greater ratios would be expected.

VIII. TITANIUM-SILVER CONTACTS

An attempt was made to fabricate cells with titanium-silver contacts. These contacts are reported to make a better ohmic contact than aluminum ("Electrochemically Passivated Contacts for Silicon Solar Cells," H. Fischer and R. Gereth, IEEE Trans. Elec. Dev., Vol. ED-18, No. 8, Aug. 1971, pp. 459). The low curve factor of the inversion layer cell with aluminum contacts is partially due to the high resistance of the contacts. Therefore, the successful deposition of Ti-Ag is important to produce a more efficient cell.

The titanium-silver was evaporated in a vacuum station with separate sources. A shutter protected the wafer from the initial evaporants and was opened after the titanium was brought to evaporation temperature. After about 600 A of titanium was deposited, the silver was heated to evaporation temperature and blended in with the titanium as the titanium evaporation was shut down. The silver evaporation continued until the desired coating was obtained.

The evaporation of the metals was successfully accomplished but the metal layers lifted from the wafer during the photo-etch processing. Many attempts to eliminate the problem of peeling were tried but each was unsuccessful. The peeling only occurred on the polished surface leaving the bottom surface with a good adherent-ohmic contact. An experiment was performed on a blank wafer whereby a disk of Ti-Ag equal in area to the finger pattern was evaporated through a mask on the polished surface and the normal evaporation on the bottom surface. The wafer was sintered at 600°C for three minutes after removing it from the vacuum station. No wet chemicals touched the surface as would occur during the photo-etch process. The contact was very adherent to the surface with no evidence of peeling and was impervious to

solvent and water washes. The resistance from front to back on the contact areas was .94 ohms. A calculation of the resistance, assuming a 10 ohm-cm wafer, indicates the resistance should be about .91 ohms. Thus, it can be assumed that a good ohmic contact is formed using the sintered titanium-silver deposition.

Another evidence that a good contact can be obtained with the Ti-Ag contacts, if no wet process is involved before sintering, is the successful fabrication of a conventional p-n junction solar cell with a curve factor equal to the curve factor of a conventional manufactured cell. The finger contact was evaporated through a mask. This indicates a good low resistance contact. Comparative curves of a manufactured cell and a conventional cell fabricated in the lab is found in Fig. 40. No antireflection SiO coating was used on the latter cell.

Because of the difficulty of processing inversion layer cells with titanium-silver contacts, cells with this contact were not fabricated.

IX. CONCLUSIONS

It has been experimentally shown that an induced p-n junction can act as a collector of free charges in a semiconductor that have been created by photons. Thus, a photovoltaic cell can be produced by creating an inversion layer near the surface of a semiconductor and applying suitable contacts to carry the electrical power to an external load. It has also been demonstrated that these cells are sensitive to the short wavelengths of the sun's spectrum.

Several ways of inducing this junction have been illustrated such as use of a transparent conducting coating separated from the semiconductor by an insulator, an oxide on the surface of the semiconductor containing ions from contaminants purposely placed there and providing surface states that act as equivalent donors to the surface of the semiconductor.

X. RECOMMENDATIONS OF FUTURE INVESTIGATION

1. That this cell be fabricated with Ti-Ag contacts with the aid of the expertise and experience of a solar cell manufacturer.

2. That further optimization of the grid structure be performed to increase the efficiency and curve factor of the cell.

3. That the contaminated oxide cell be explored further with respect to different contaminants and other insulating layers.

4. That the transparent electrode cell be explored further to increase the efficiency.

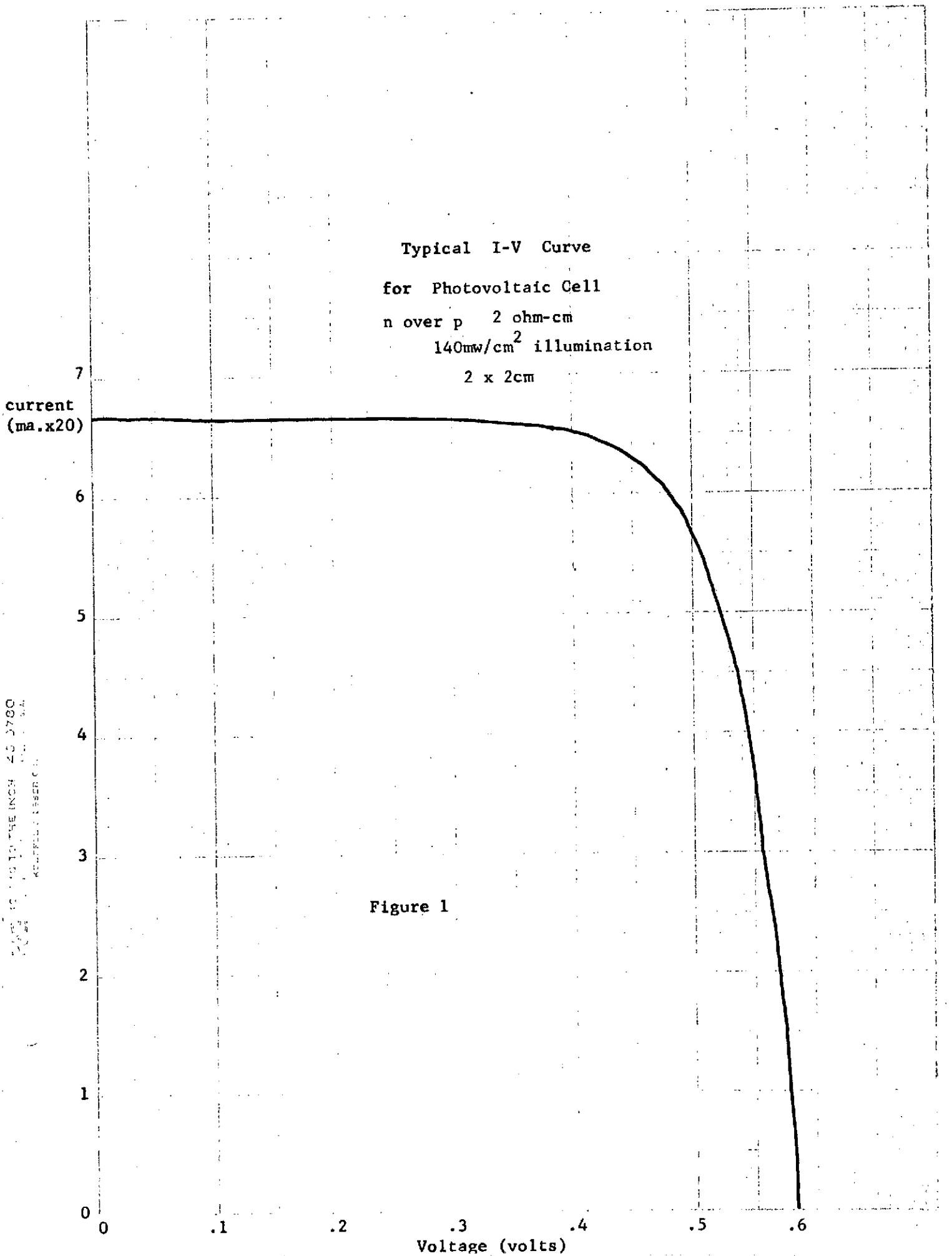
Typical I-V Curve
for Photovoltaic Cell
n over p 2 ohm-cm
140mw/cm^2 illumination
2 x 2cm
current
(ma.x20)
7
6
5
4
3
2
1
0
0
.1
.2
.3
.4
.5
.6
Voltage (volts)

Figure 1

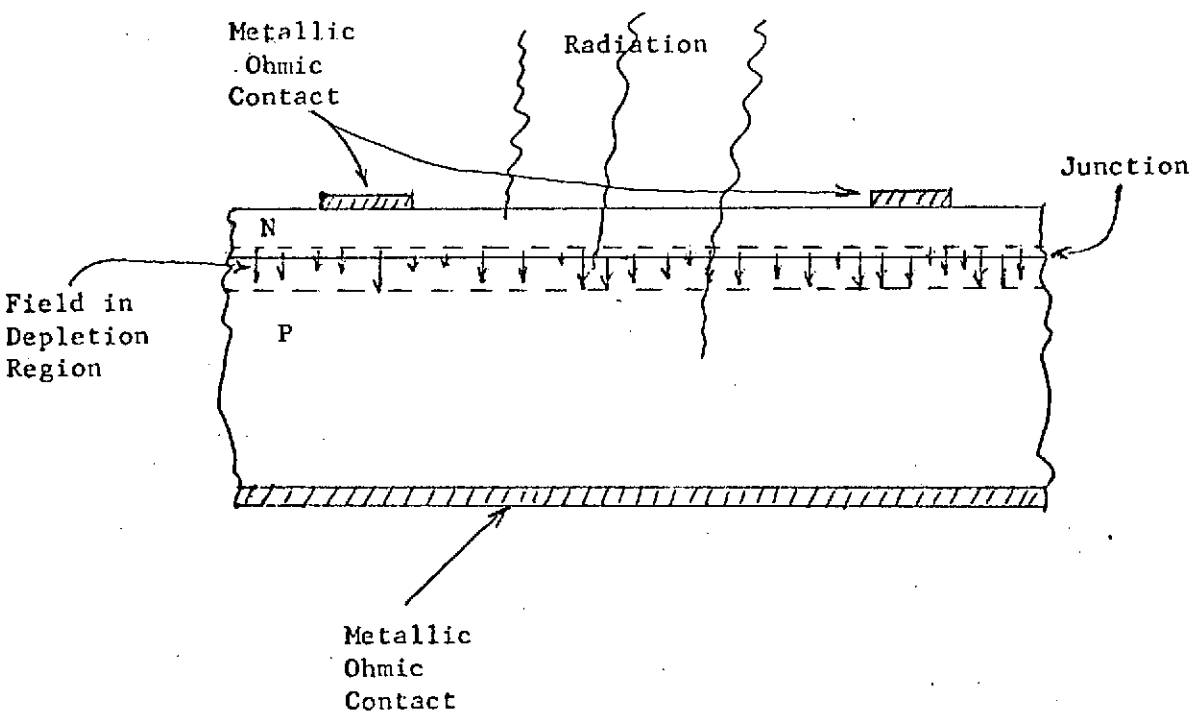

Figure 2.

Standard Solar Cell Construction

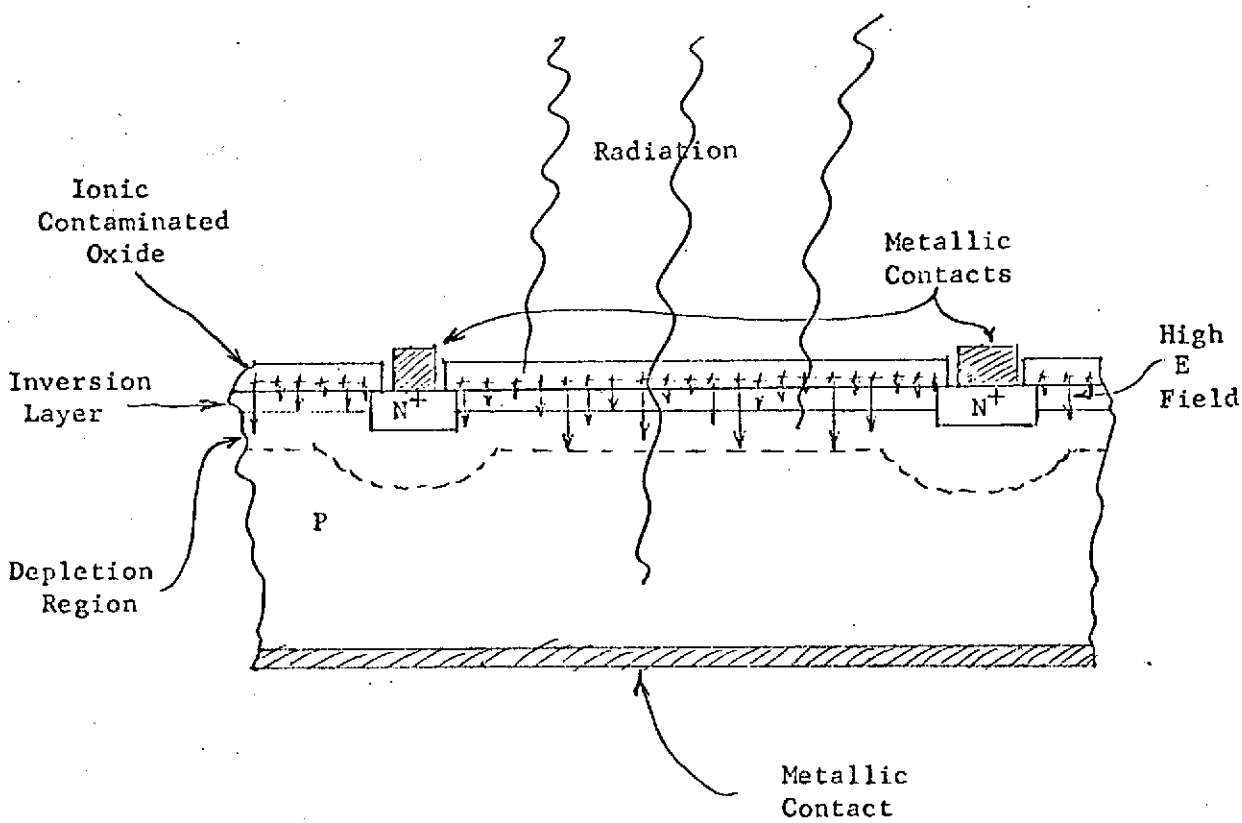

Figure 3

Inversion Layer Solar Cell

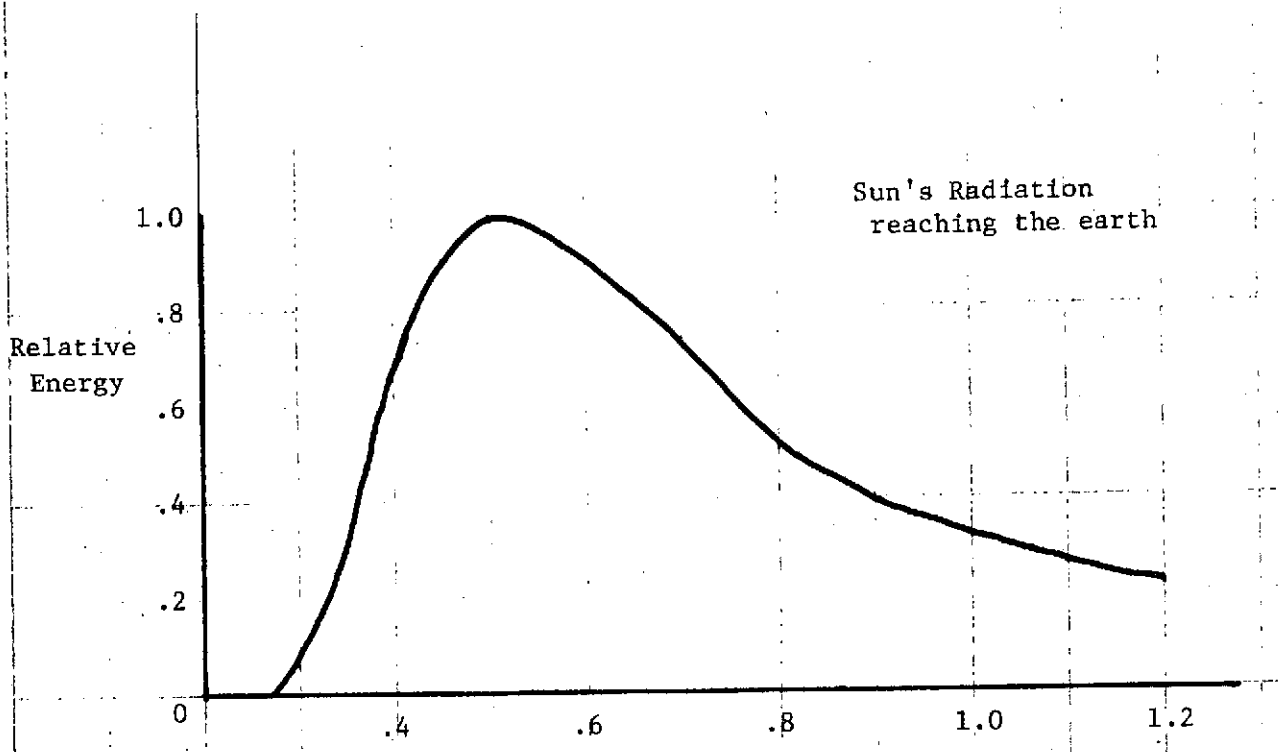

Figure 4a

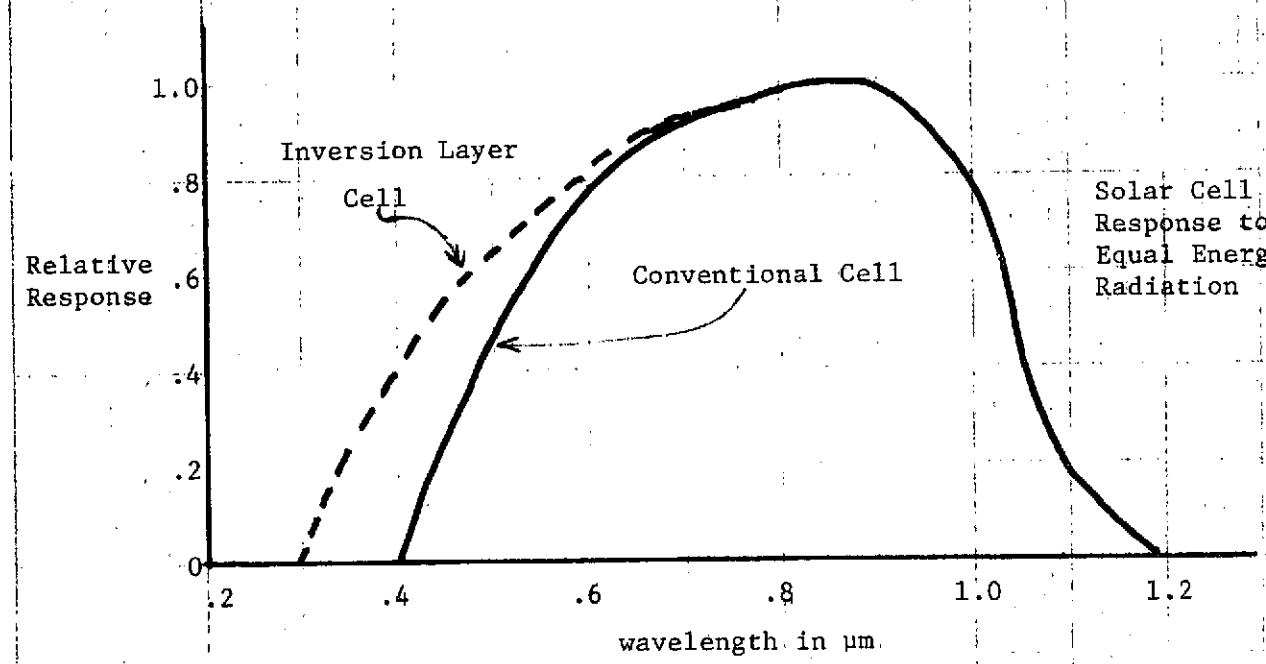

Figure 4b

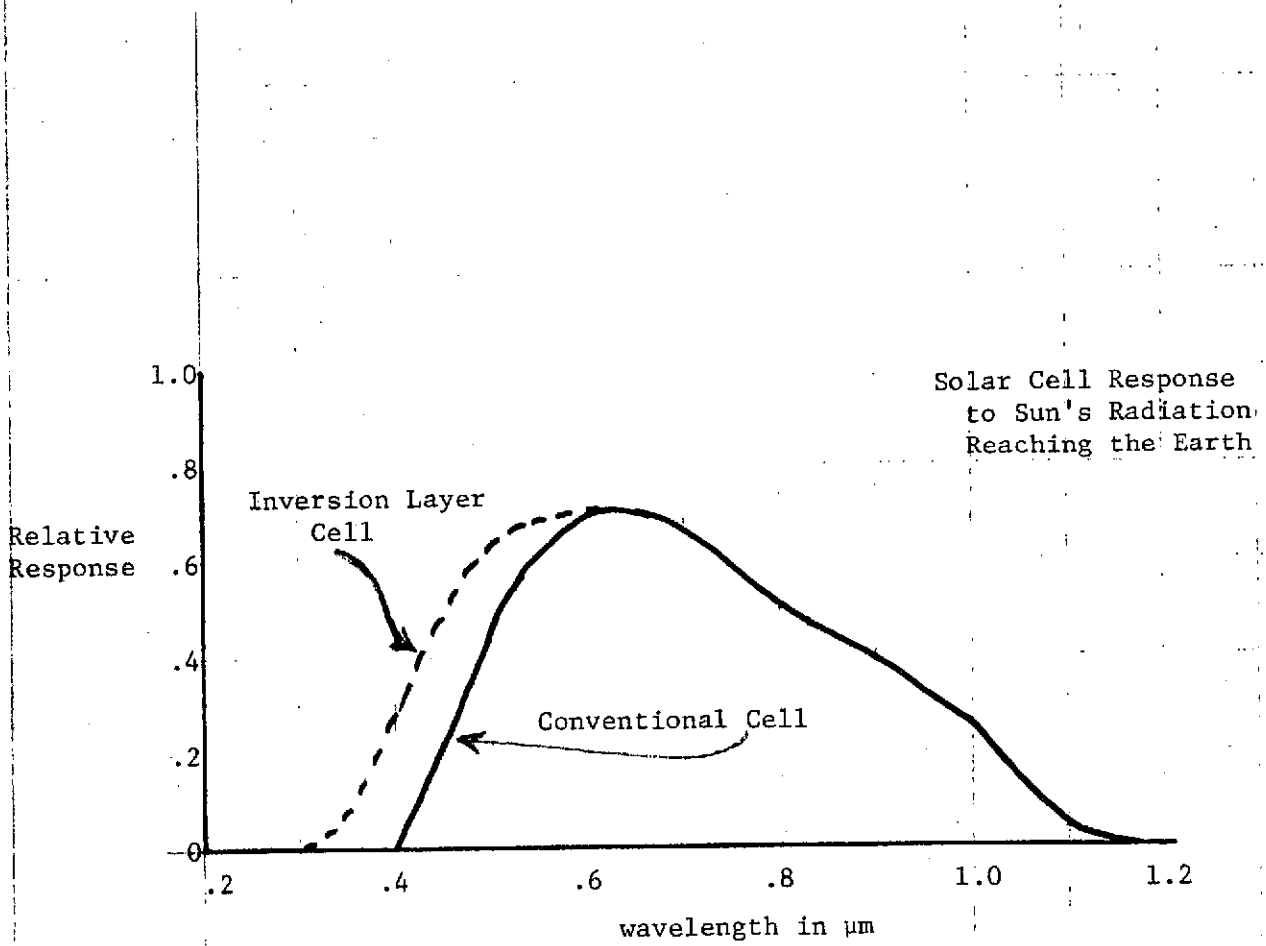
Solar Cell Response
to Sun's Radiation
Reaching the Earth
Relative
Response
1.0
.8
.6
.4
.2
0
Inversion Layer
Cell
Conventional Cell
.2
.4
.6
.8
1.0
1.2
wavelength in μm

Figure 5

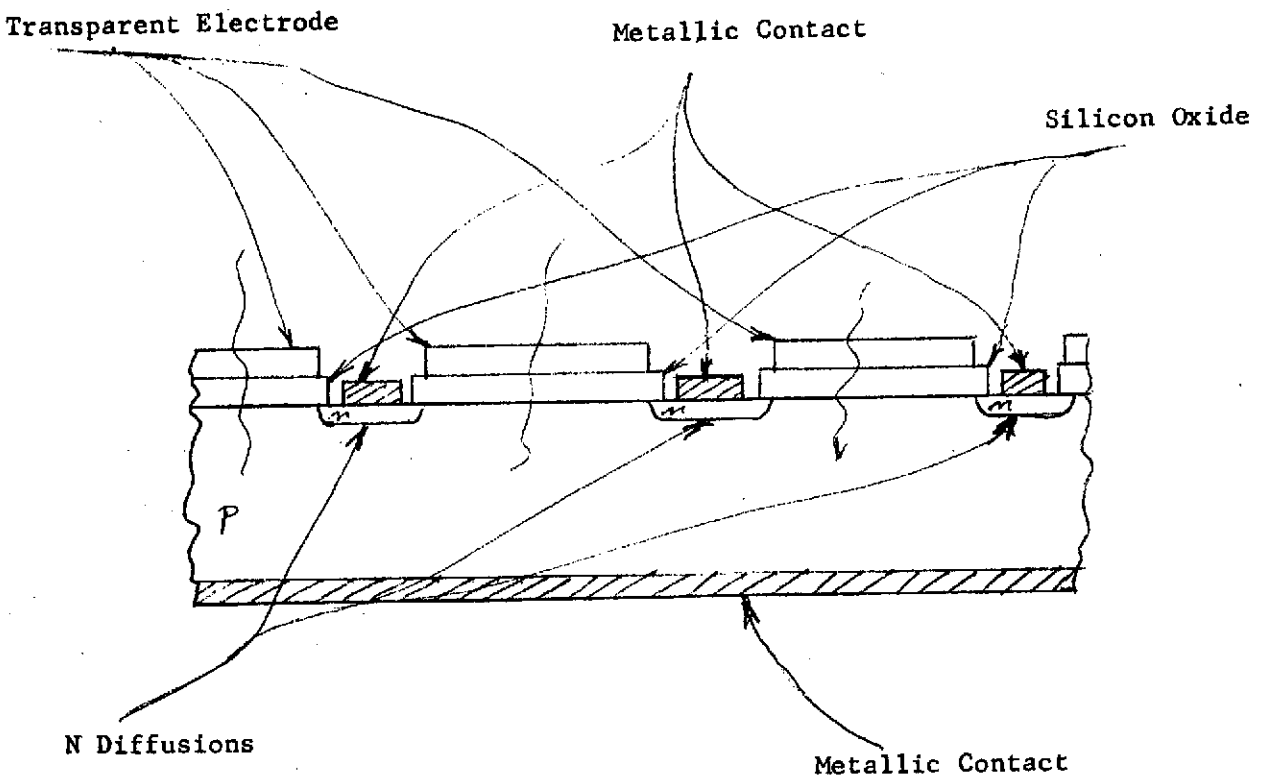

Figure 6

Transparent Electrode Cell

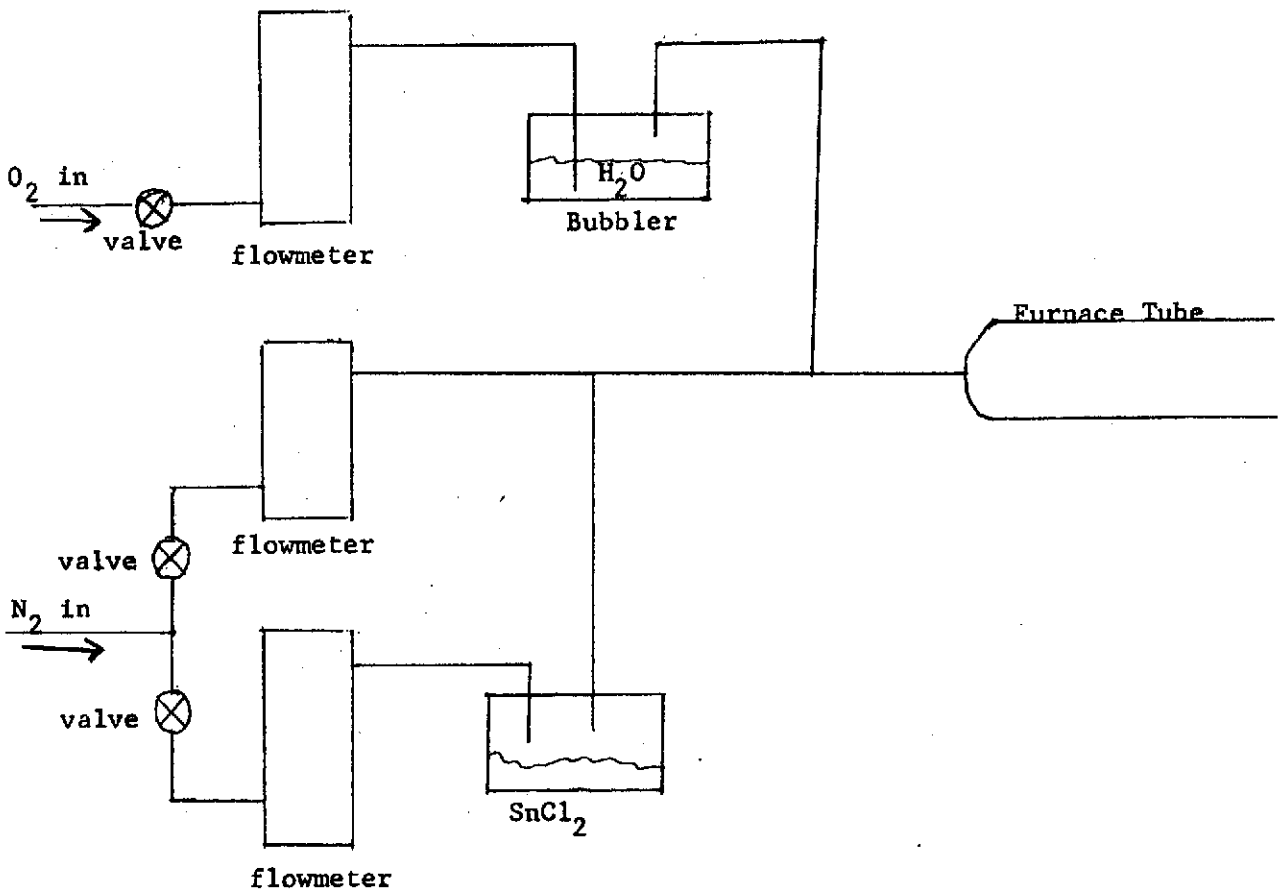

Apparatus for Depositing Tin Oxide
(the transparent electrode)

Figure 7

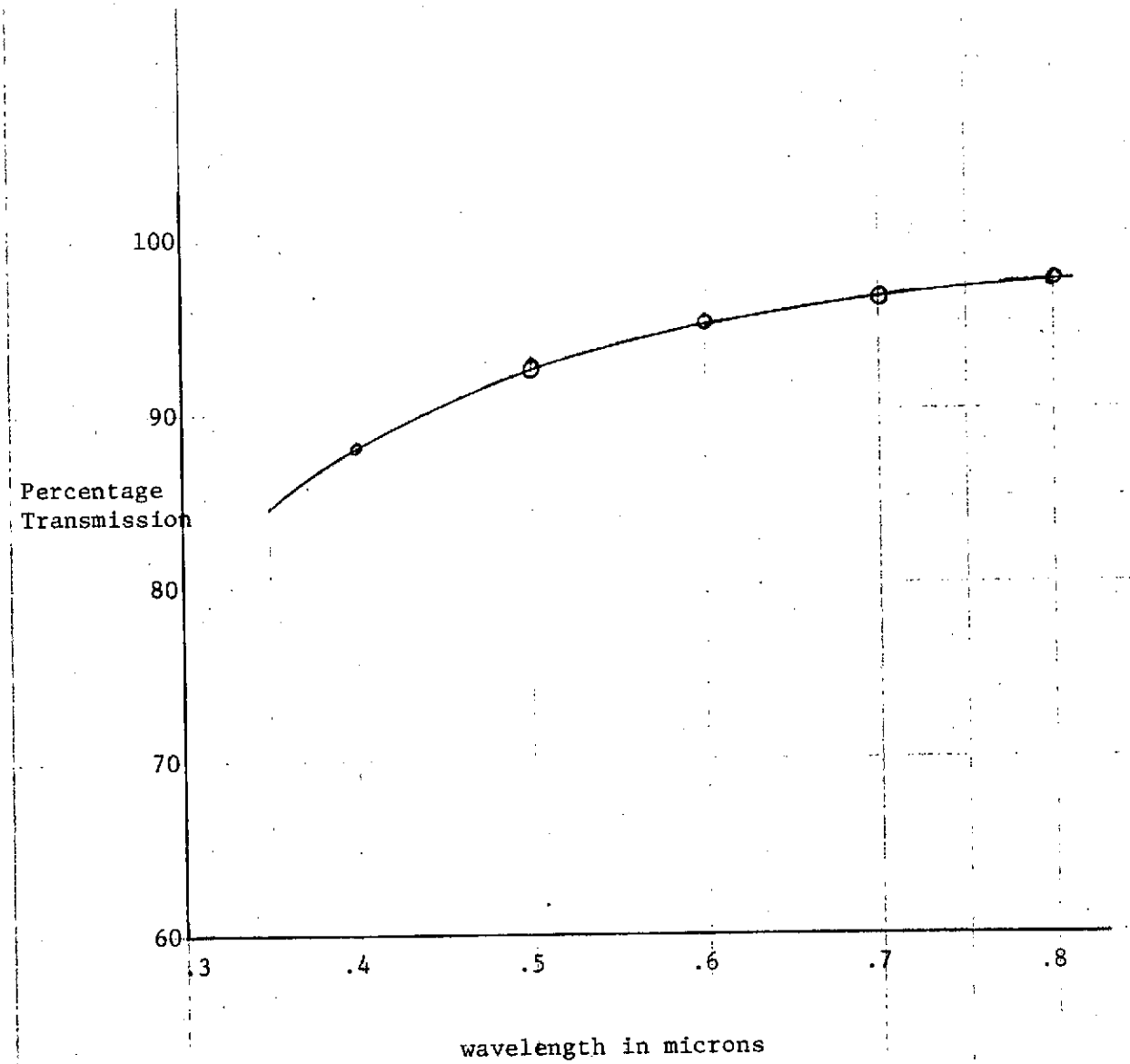

Figure 8 Optical Transmission Characteristics of a Typical Tin Oxide Layer

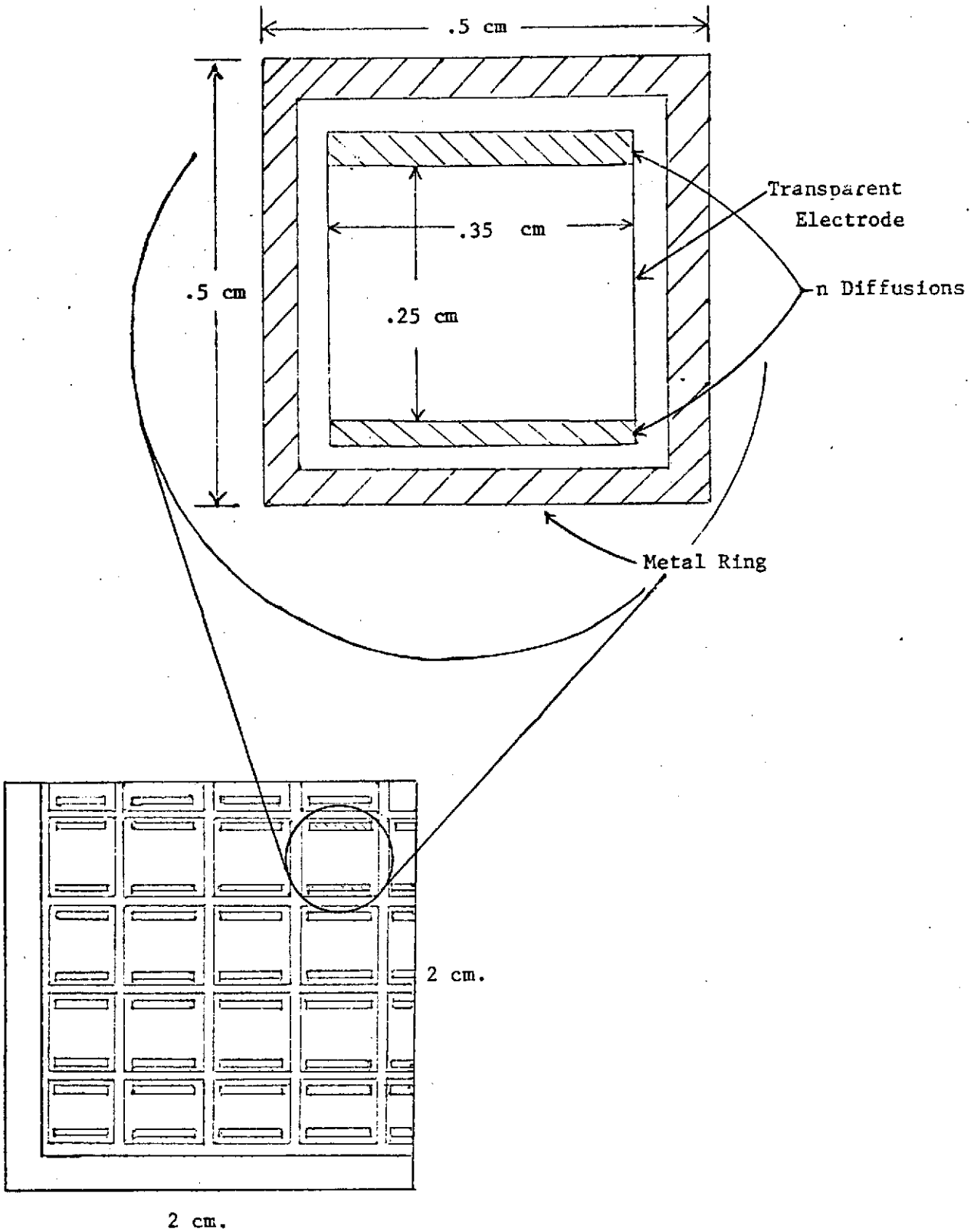

Figure 9

New Cell Configuration

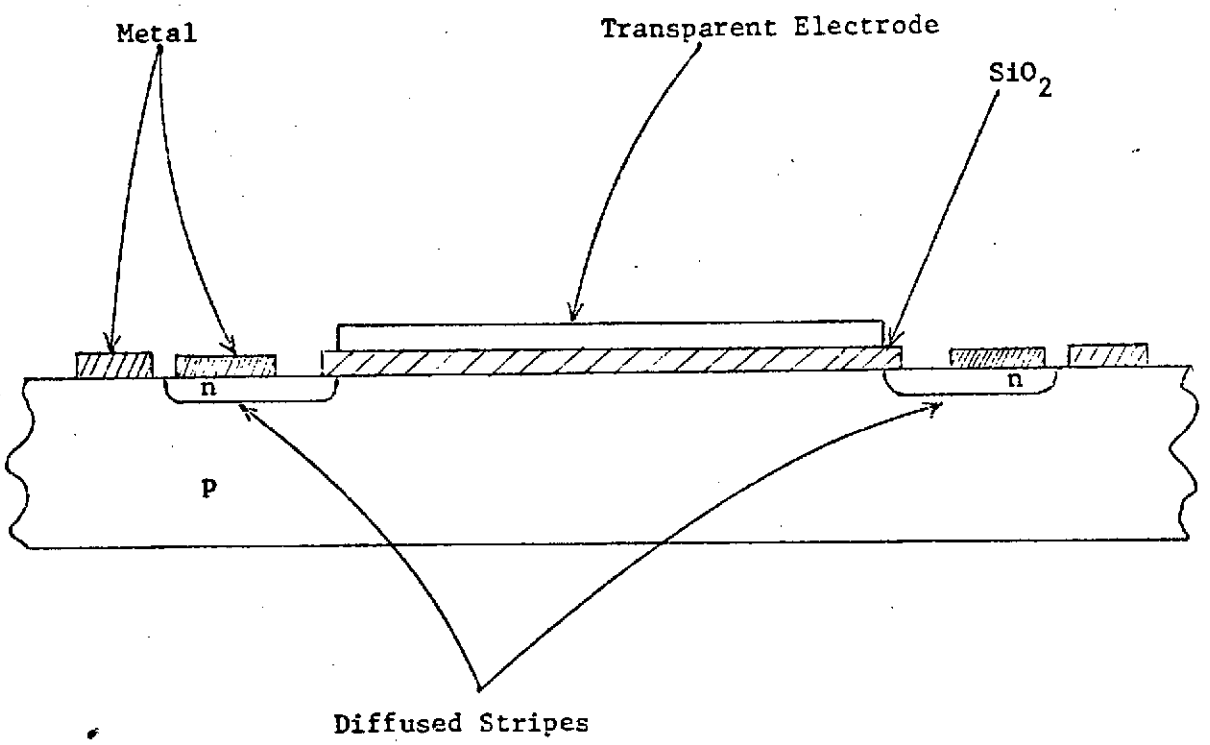

Figure 10

Cross-section of New Cell Configuration

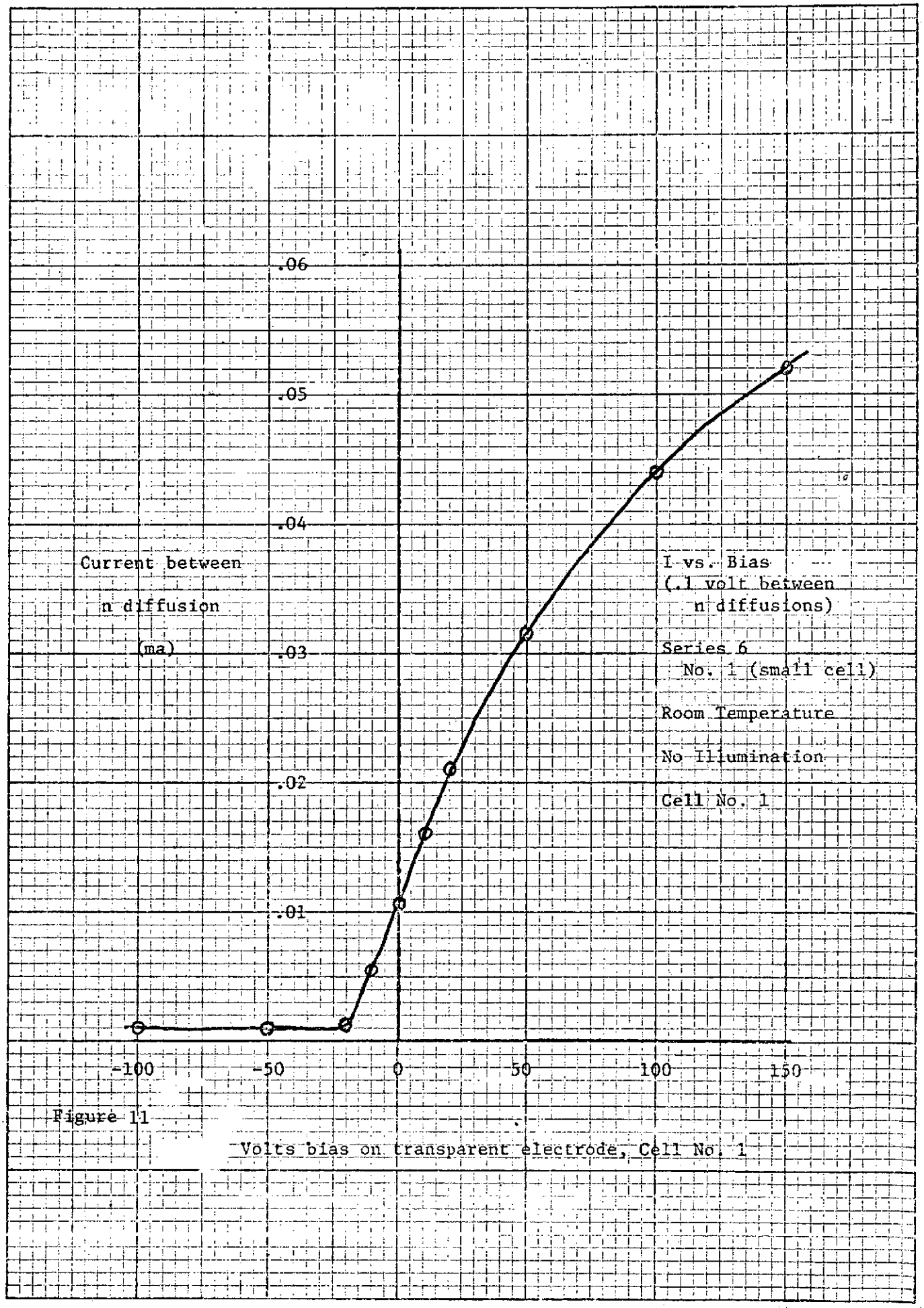

Figure 11

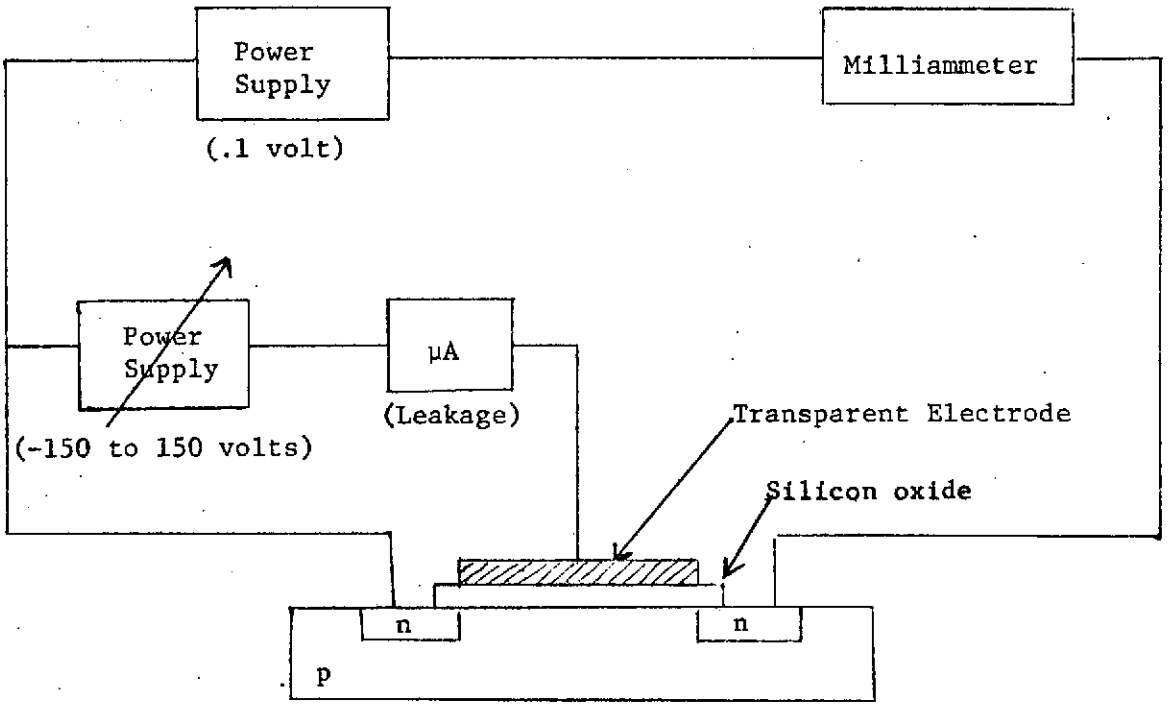

Figure 12

Circuit Used for Conductance Measurements

Figure 13

Transparent electrode bias vs. I_{sc} for small cell, series 6, wafer 1.

FBE Lamp source
100mw/cm^2

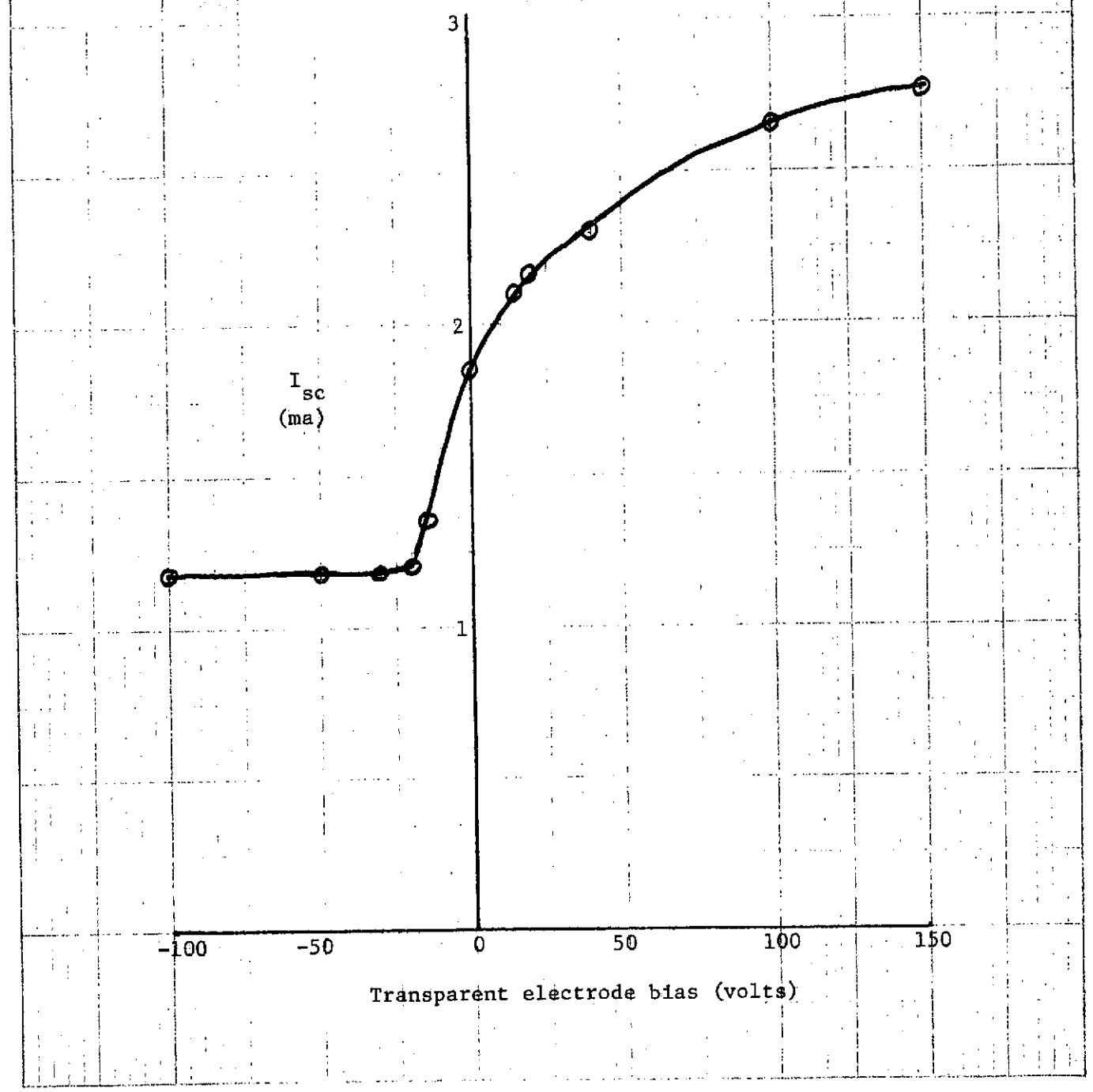

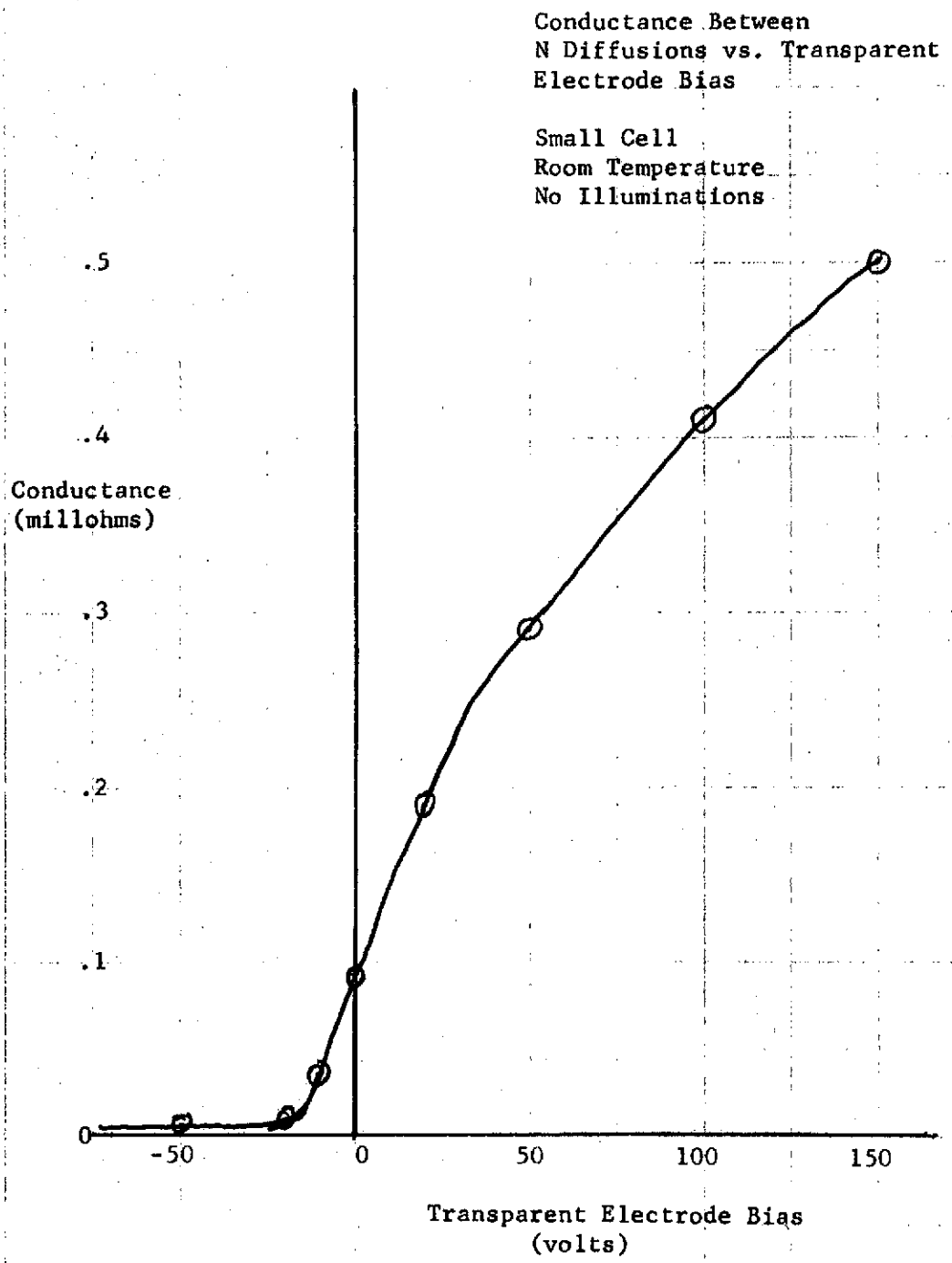
Conductance Between
N Diffusions vs. Transparent
Electrode Bias
Small Cell
Room Temperature
No Illuminations
.5
.4
Conductance
(millohms)
.3
.2
.1
0
-50
0
50
100
150
Transparent Electrode Bias
(volts)

Figure 14

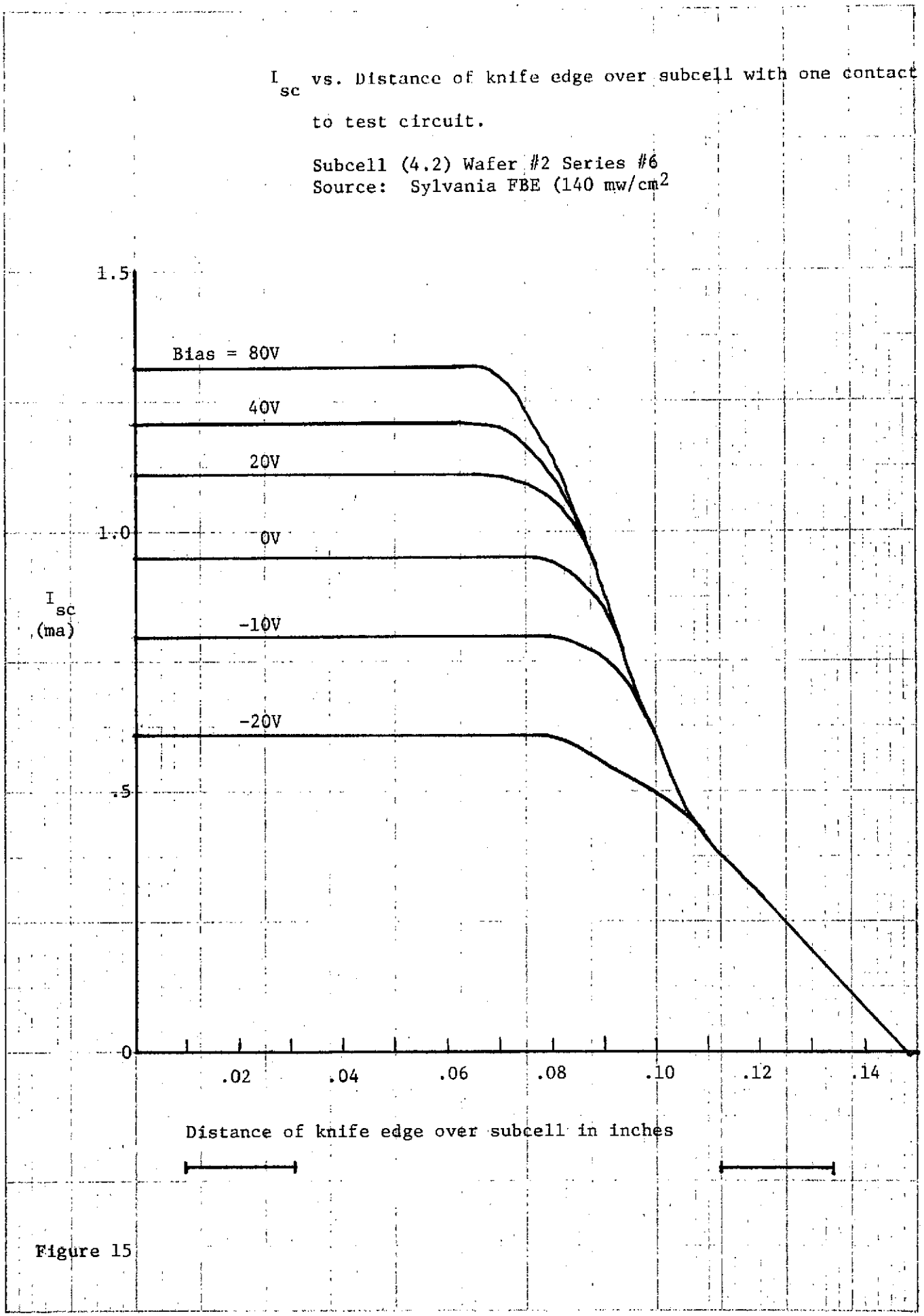
I_{sc} vs. Distance of knife edge over subcell with one contact to test circuit.
Subcell (4.2) Wafer #2 Series #6
Source: Sylvania FBE (140 mw/cm^2
1.5
1.0
.5
0
Bias = 80V
40V
20V
0V
-10V
-20V
I_{sc} (ma)
.02
.04
.06
.08
.10
.12
.14
Distance of knife edge over subcell in inches

Figure 15

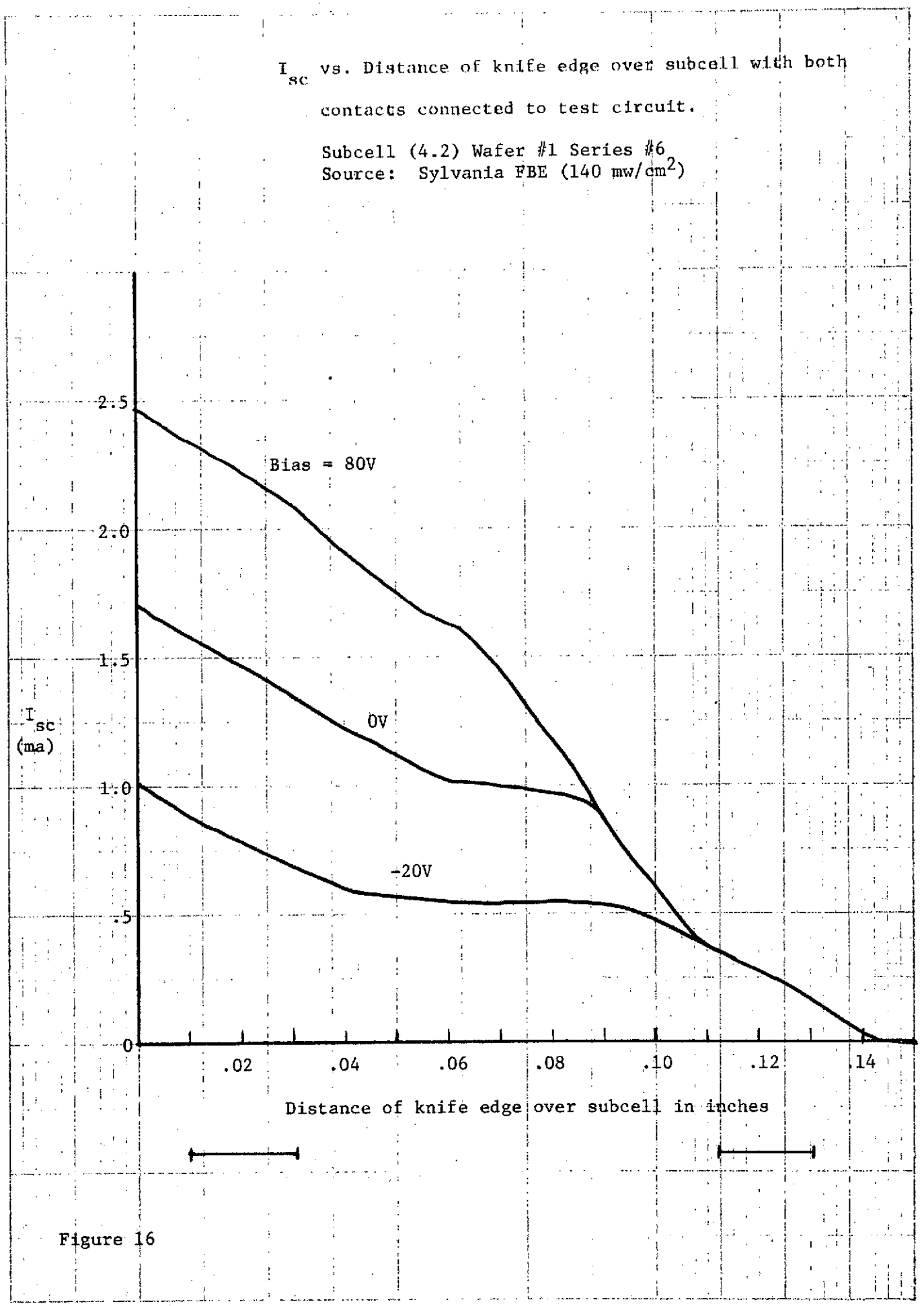
I_{sc} vs. Distance of knife edge over subcell with both contacts connected to test circuit.
Subcell (4.2) Wafer #1 Series #6
Source: Sylvania FBE (140 mw/cm^2)
Bias = 80V
0V
-20V
I_{sc} (ma)
2.5
2.0
1.5
1.0
.5
0
.02
.04
.06
.08
.10
.12
.14
Distance of knife edge over subcell in inches

Figure 16

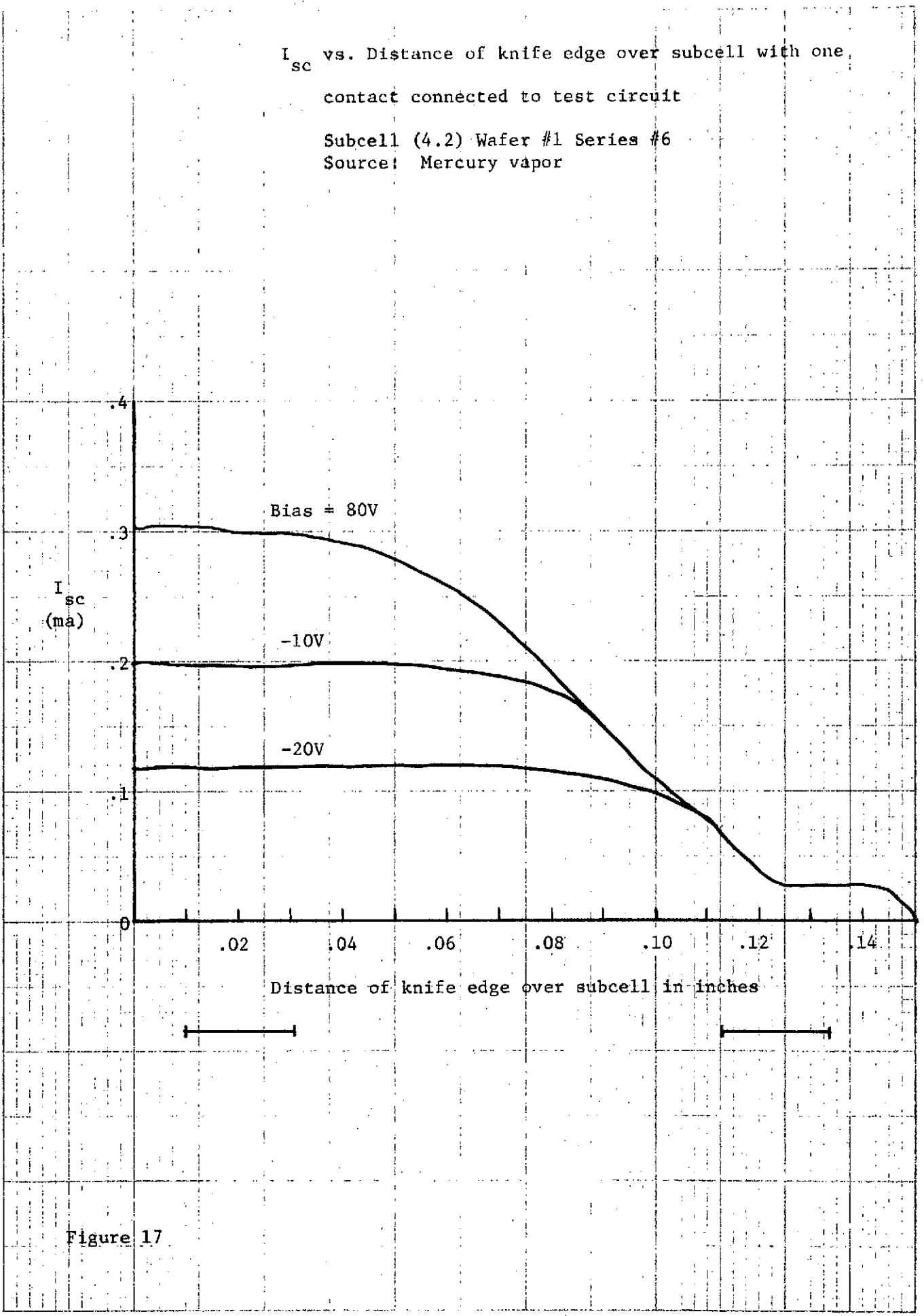
I_{sc} vs. Distance of knife edge over subcell with one contact connected to test circuit
Subcell (4.2) Wafer #1 Series #6
Source: Mercury vapor
Bias = 80V
-10V
-20V
I_{sc} (ma)
.4
.3
.2
.1
0
.02
.04
.06
.08
.10
.12
.14
Distance of knife edge over subcell in inches

Figure 17

I_{sc} vs. Distance of knife edge over subcell with one contact connected to test circuit

Subcell (4.2) Wafer #1 Series #6
Source: Ultraviolet

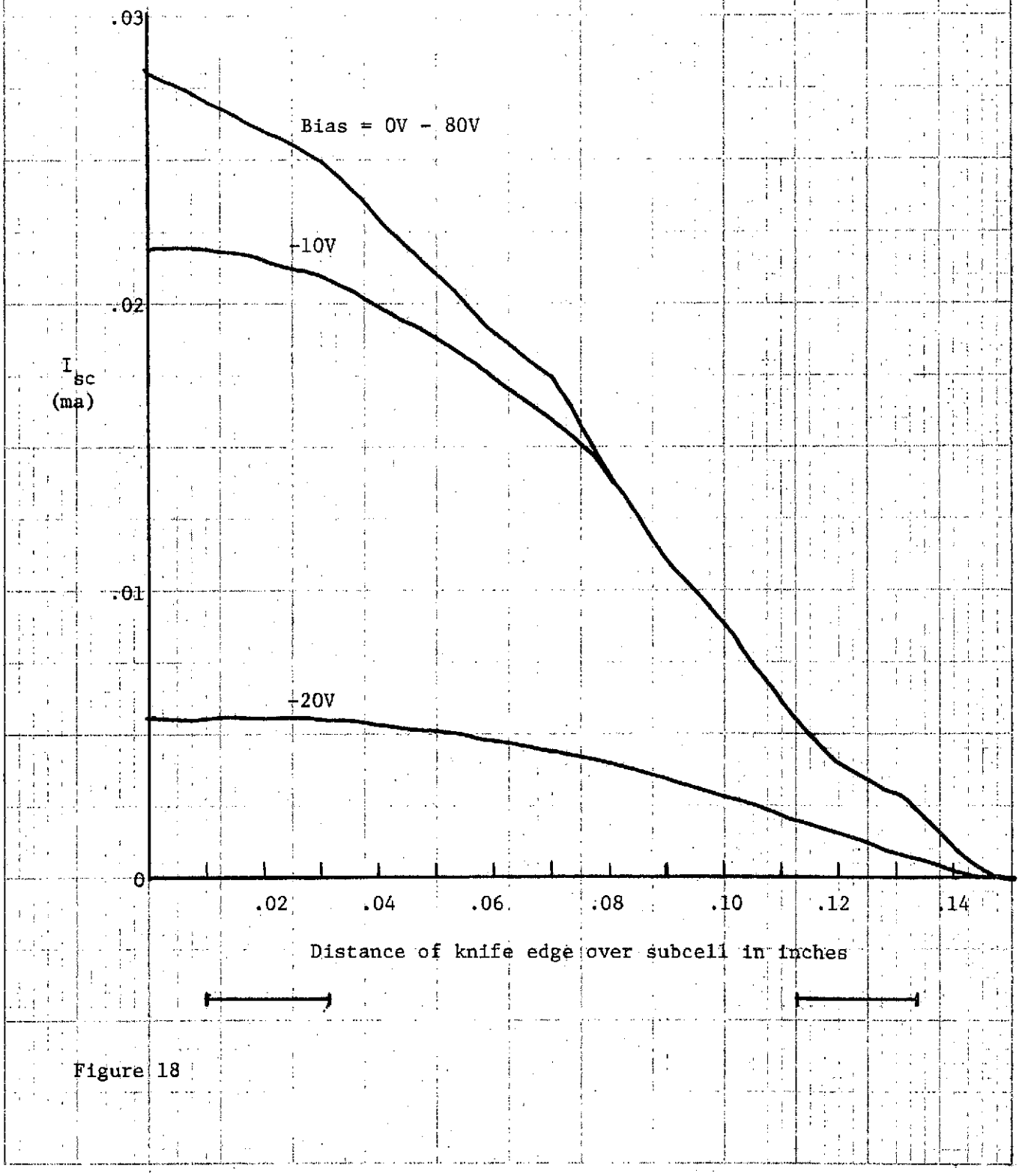

Figure 18

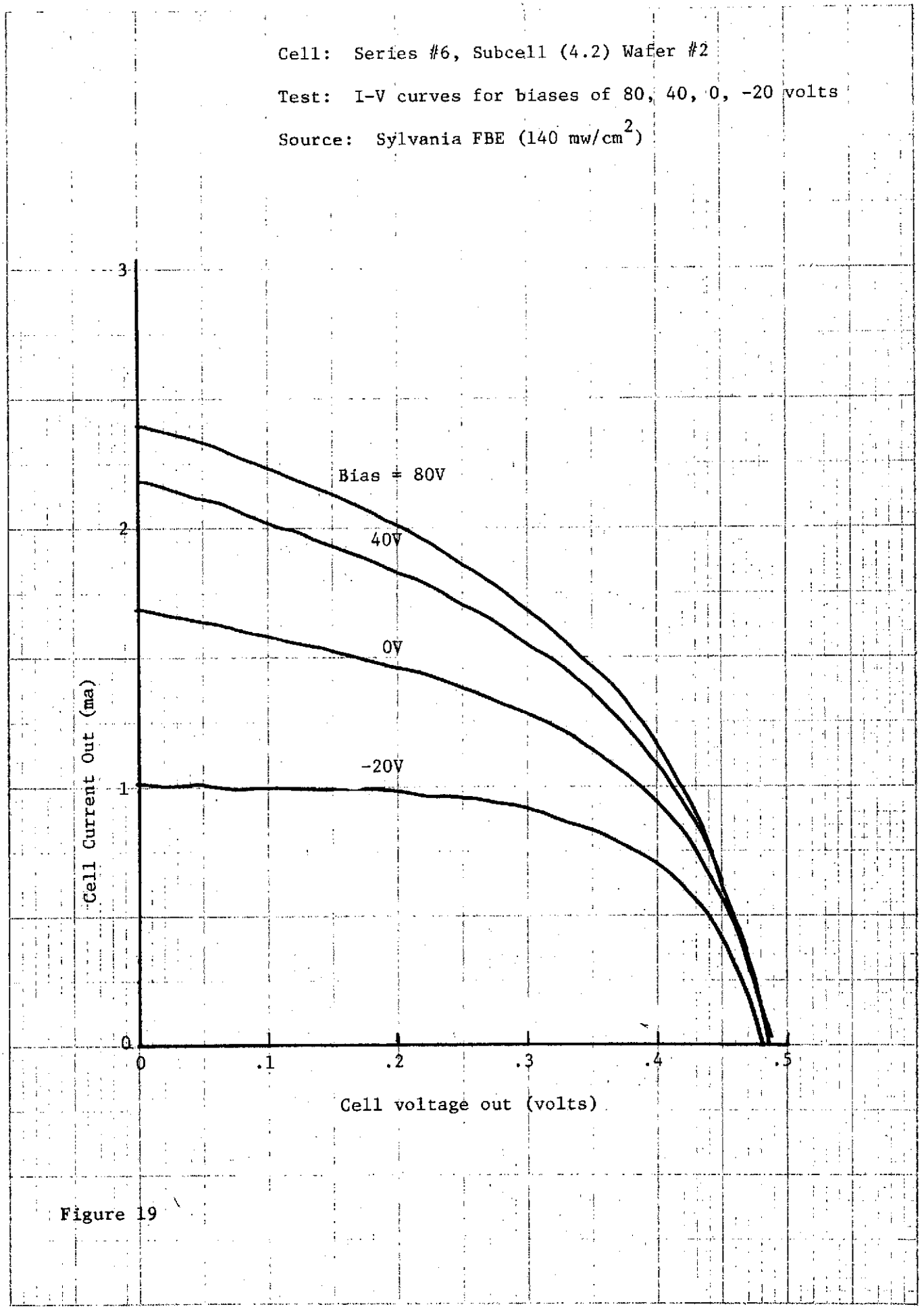
Cell: Series #6, Subcell (4.2) Wafer #2
Test: I-V curves for biases of 80, 40, 0, -20 volts
Source: Sylvania FBE (140 mw/cm^2)
Bias = 80V
40V
0V
-20V
Cell Current Out (ma)
Cell voltage out (volts)
0
1
2
3
0
.1
.2
.3
.4
.5

Figure 19

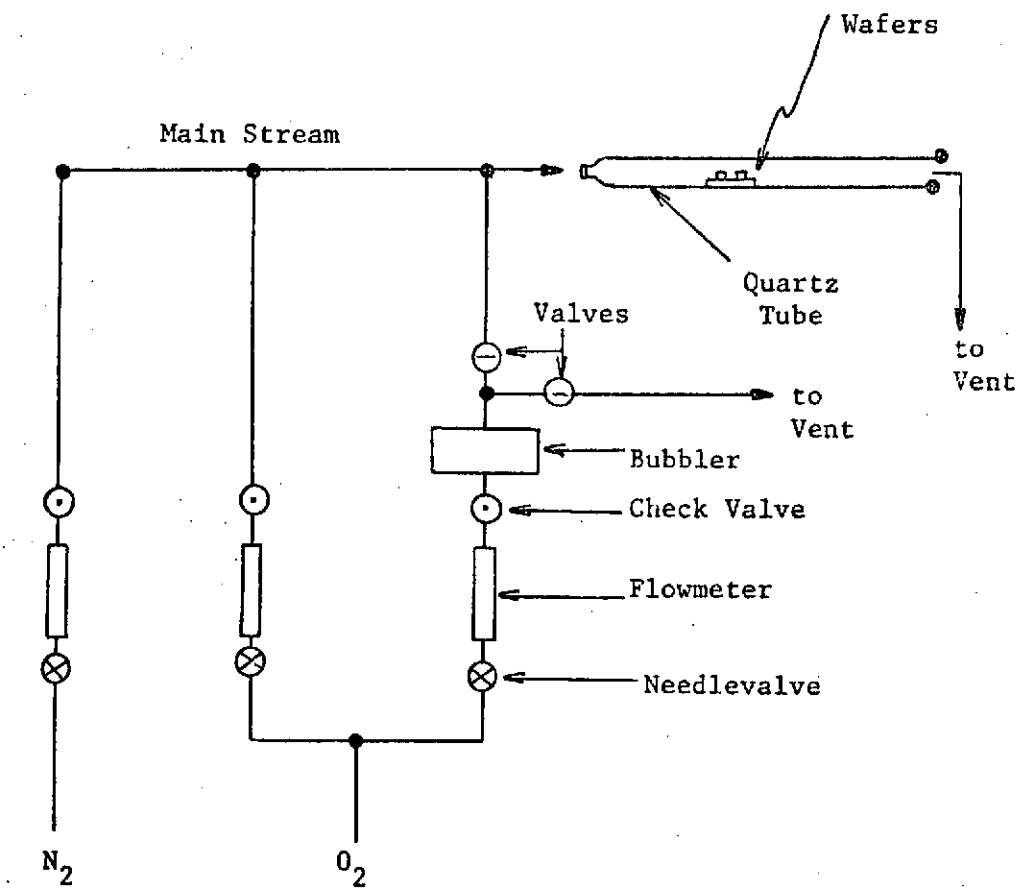

Figure 20 Schematic of Gas and Steam Supply and Vent System Used to Grow Contaminated Oxides

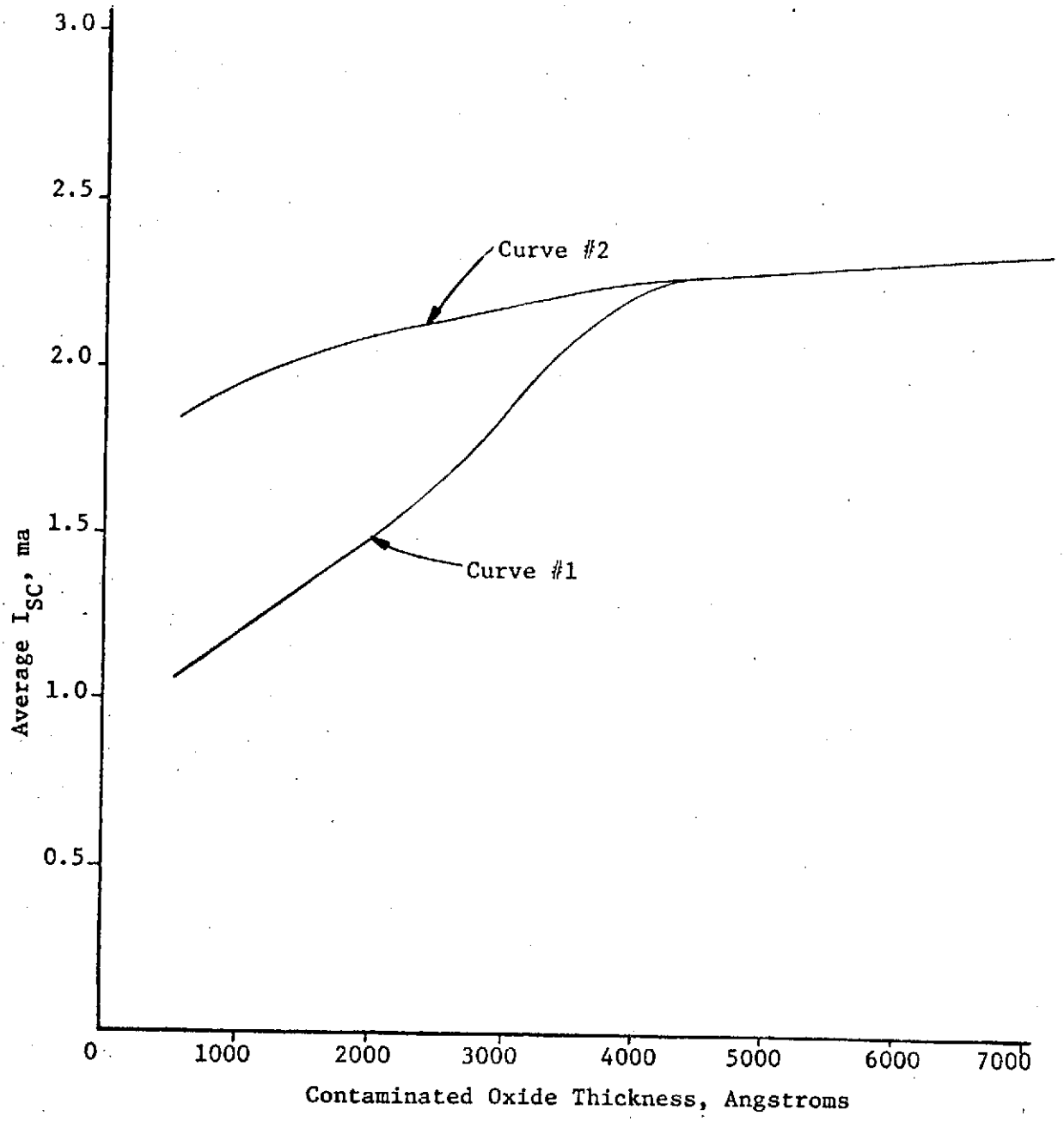

Figure 21 Plot of I_{SC} vs. Contaminated Oxide Thickness

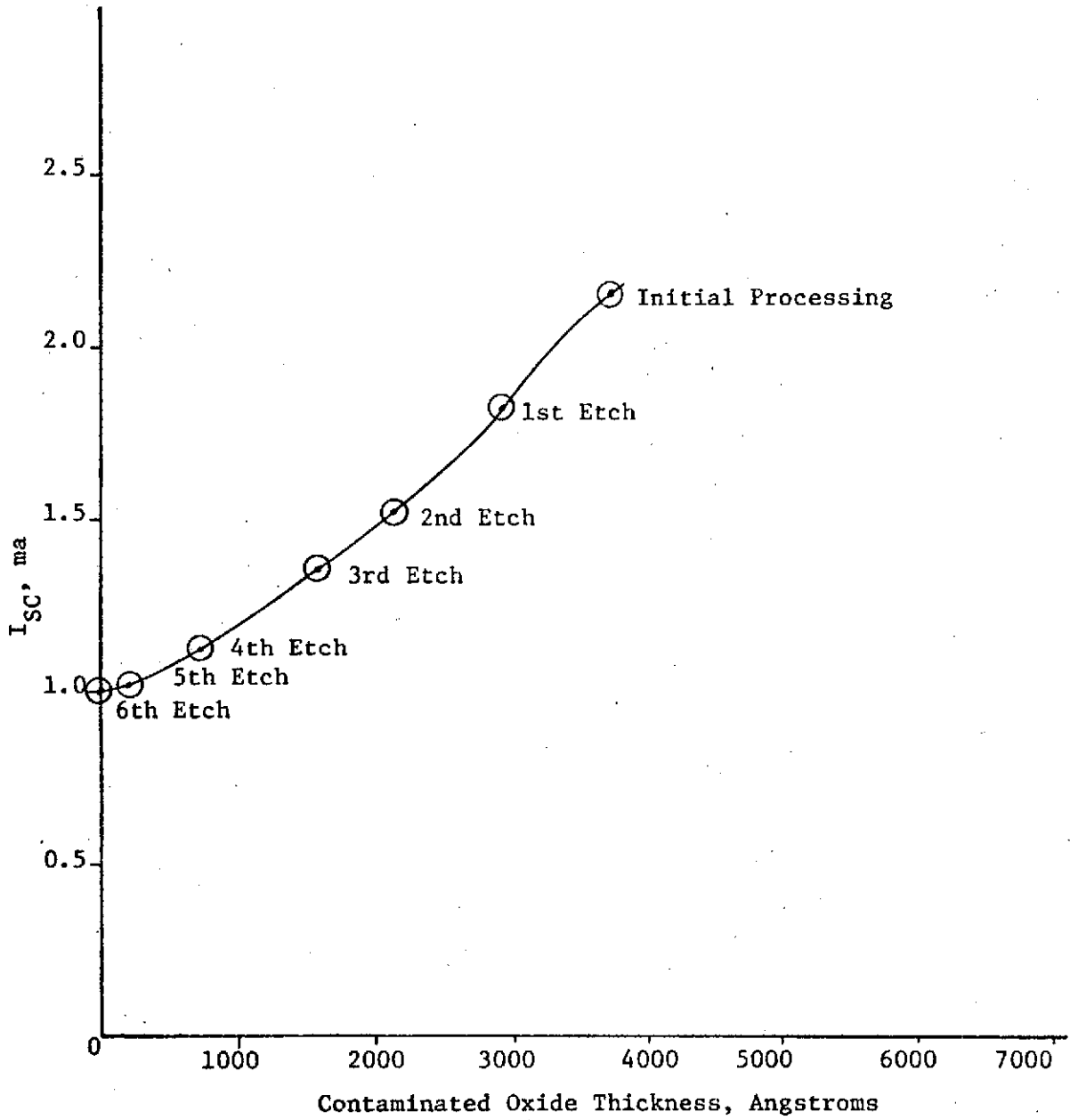

Figure 22 Plot of I_{SC} vs. Contaminated Oxide Thickness After Incremental Etching a Cell from Curve #1

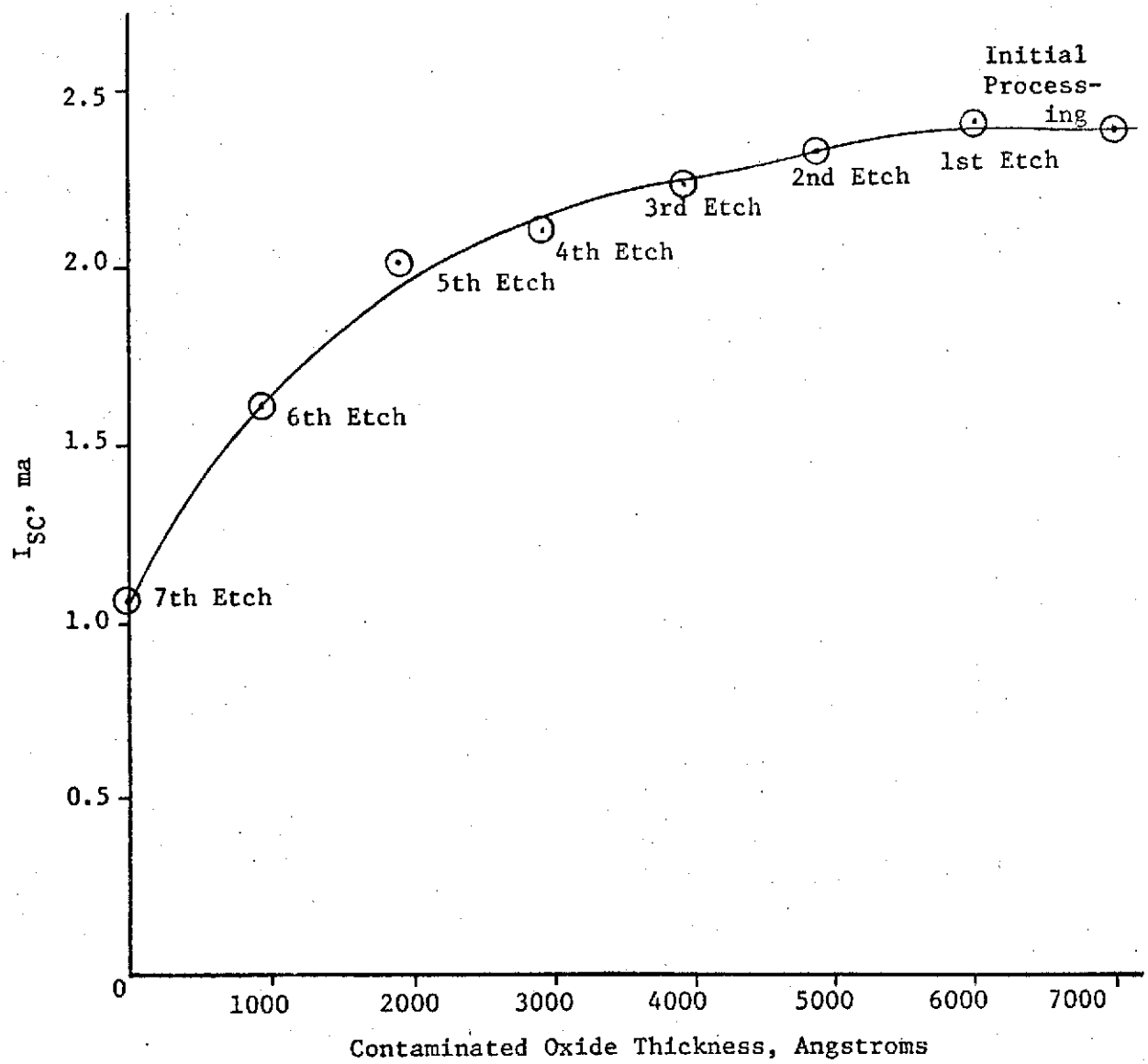

Figure 23 Plot of I_{SC} vs. Contaminated Oxide Thickness After Incremental Etching a Cell From Curve #2

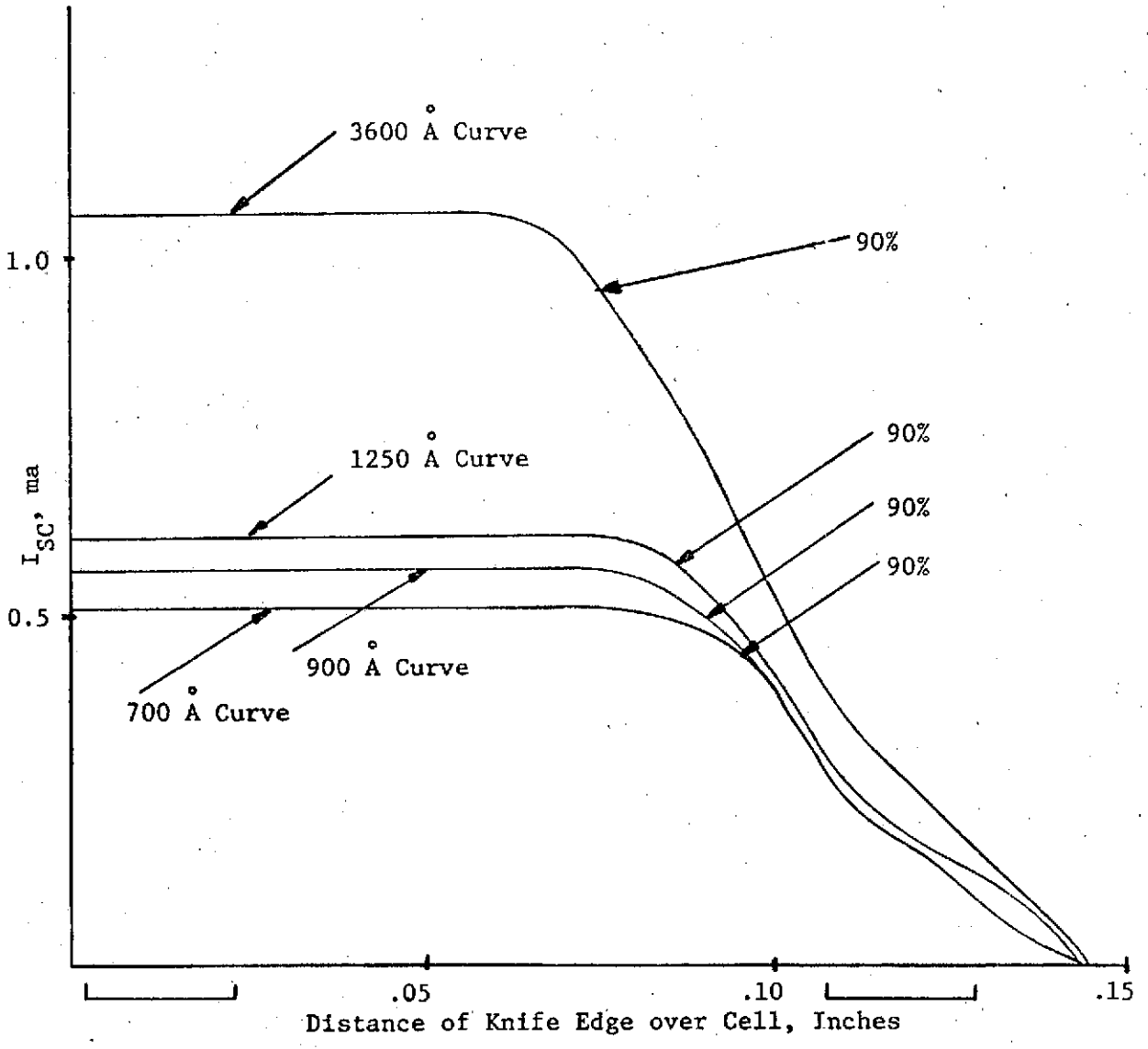

Figure 24 Plots of I_{SC} vs. Distance of Knife Edge over Cell with One Contact Connected to Test Circuit for Various Oxide Thicknesses

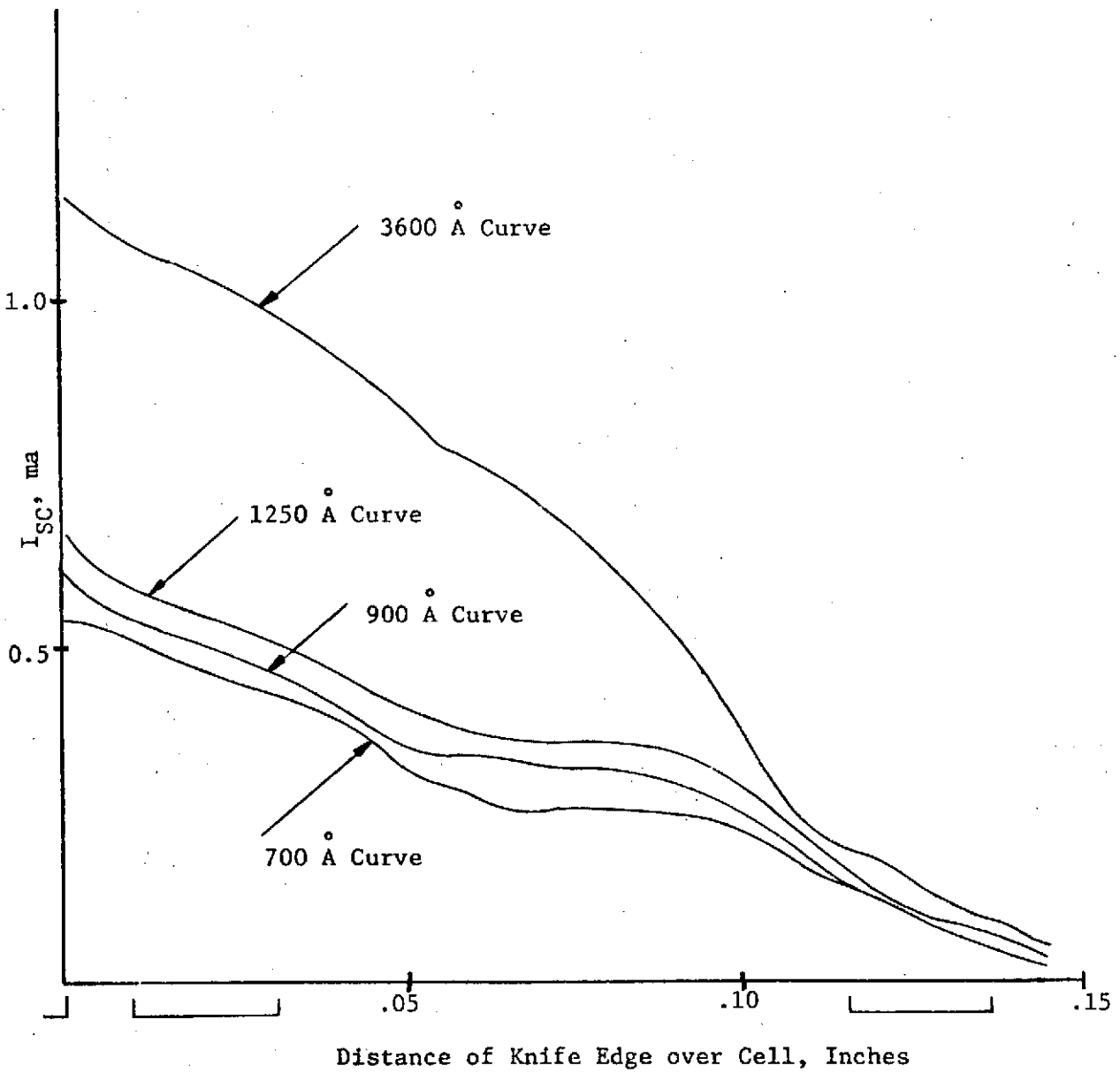

Figure 25 Plots of I_{SC} vs. Distance of Knife Edge over Cell with Both Contacts Connected to Test Circuit for Various Oxide Thicknesses

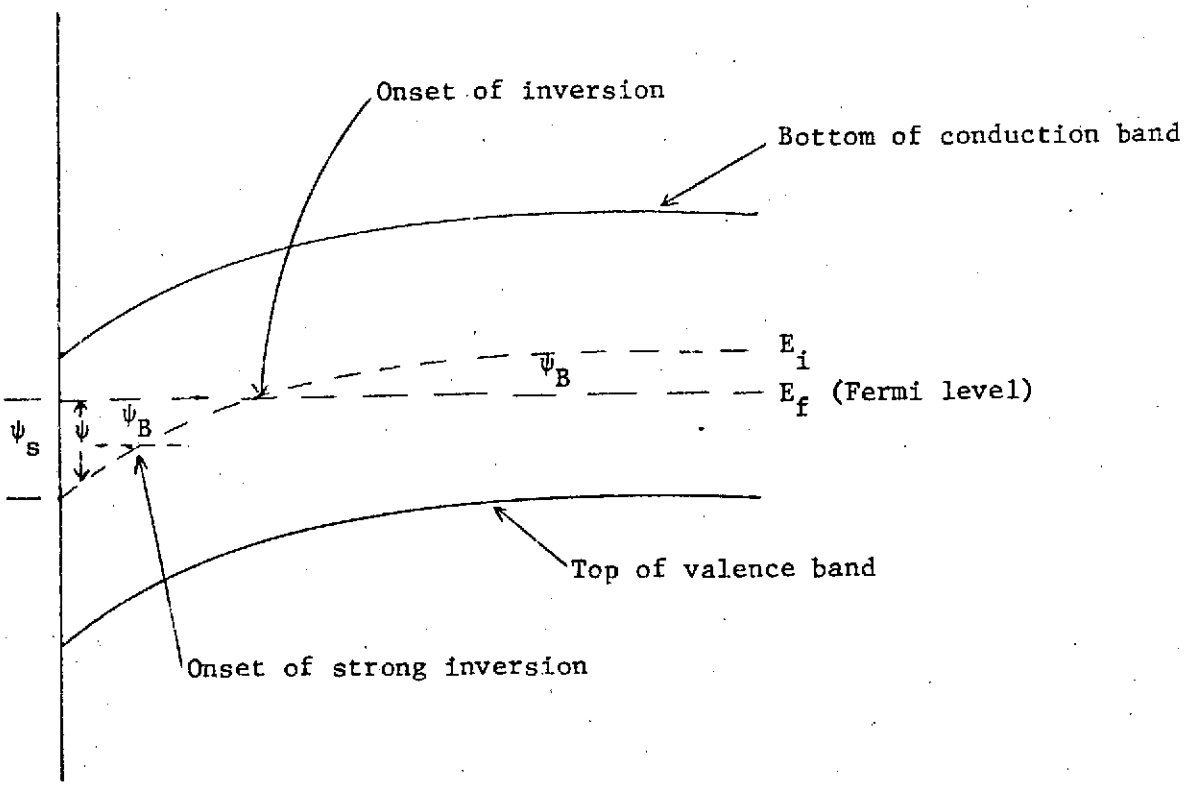

Figure 26

Band Structure of Semiconductor Surface

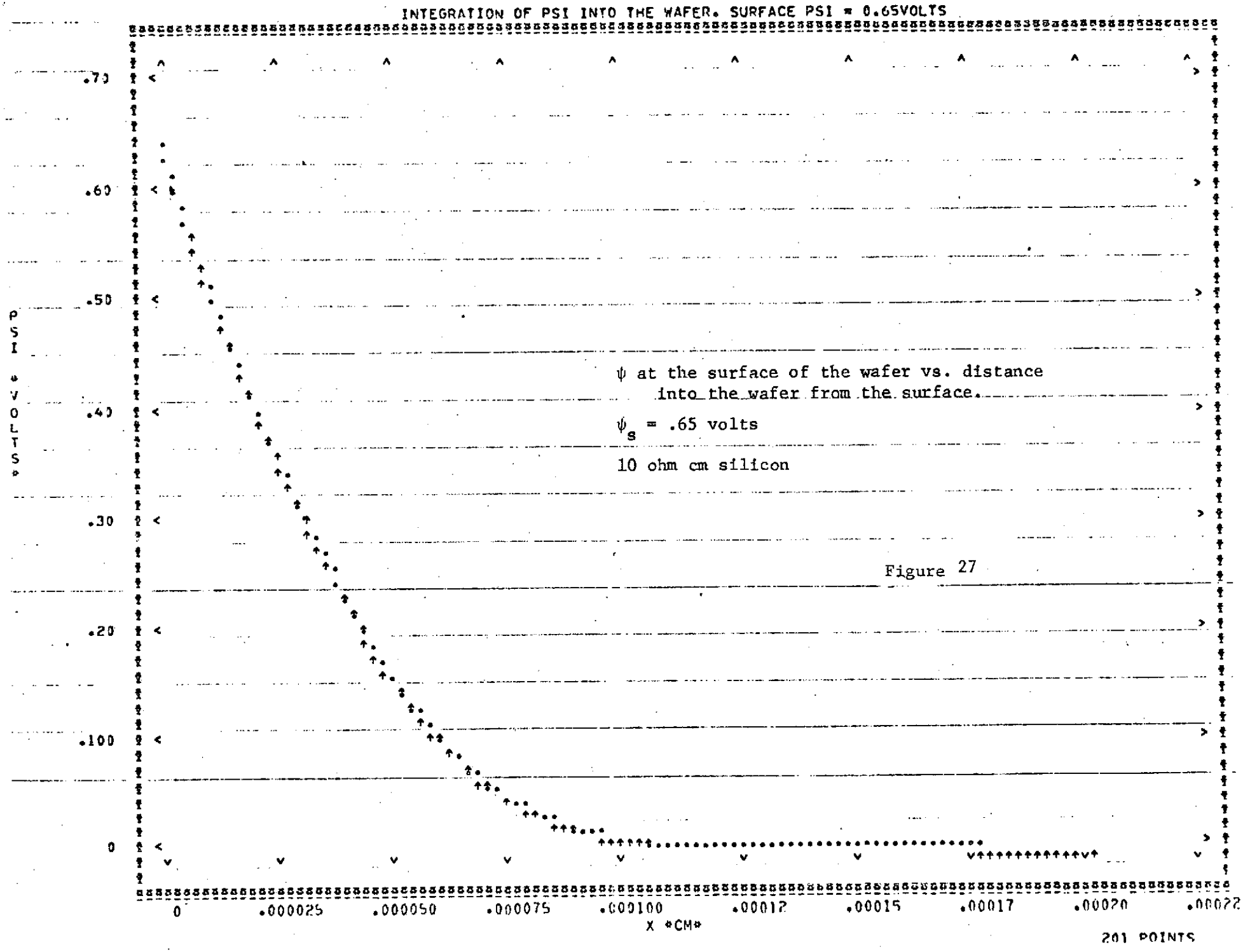
INTEGRATION OF PSI INTO THE WAFER. SURFACE PSI = 0.65VOLTS
.70
.60
.50
.40
.30
.20
.100
0
PSI *VOLTS*
ψ at the surface of the wafer vs. distance into the wafer from the surface.
ψs = .65 volts
10 ohm cm silicon
0
.000025
.000050
.000075
.000100
.00012
.00015
.00017
.00020
.00022
X *CM*
201 POINTS

Figure 27

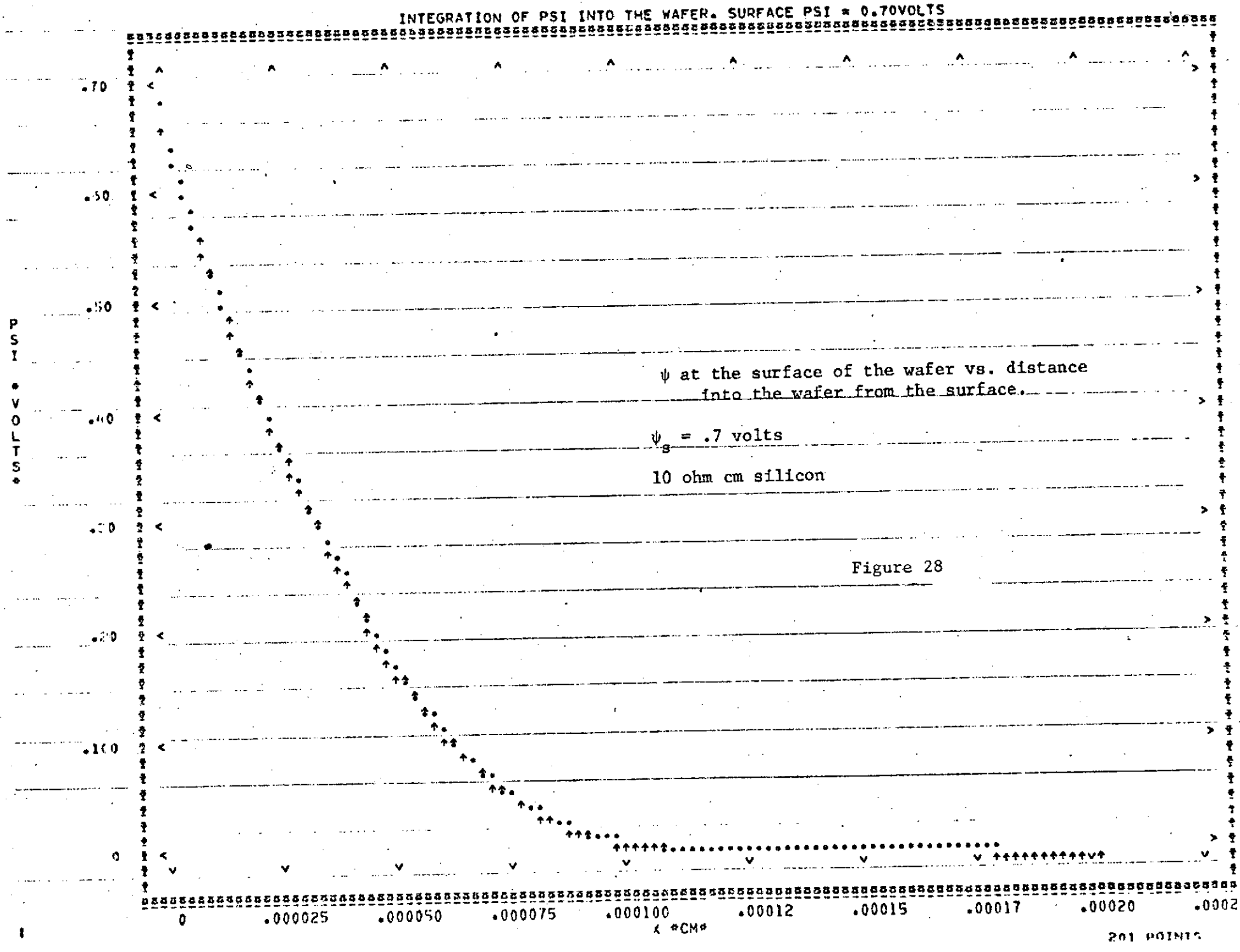

ψ at the surface of the wafer vs. distance into the wafer from the surface.

ψ_s = .7 volts

10 ohm cm silicon

Figure 28

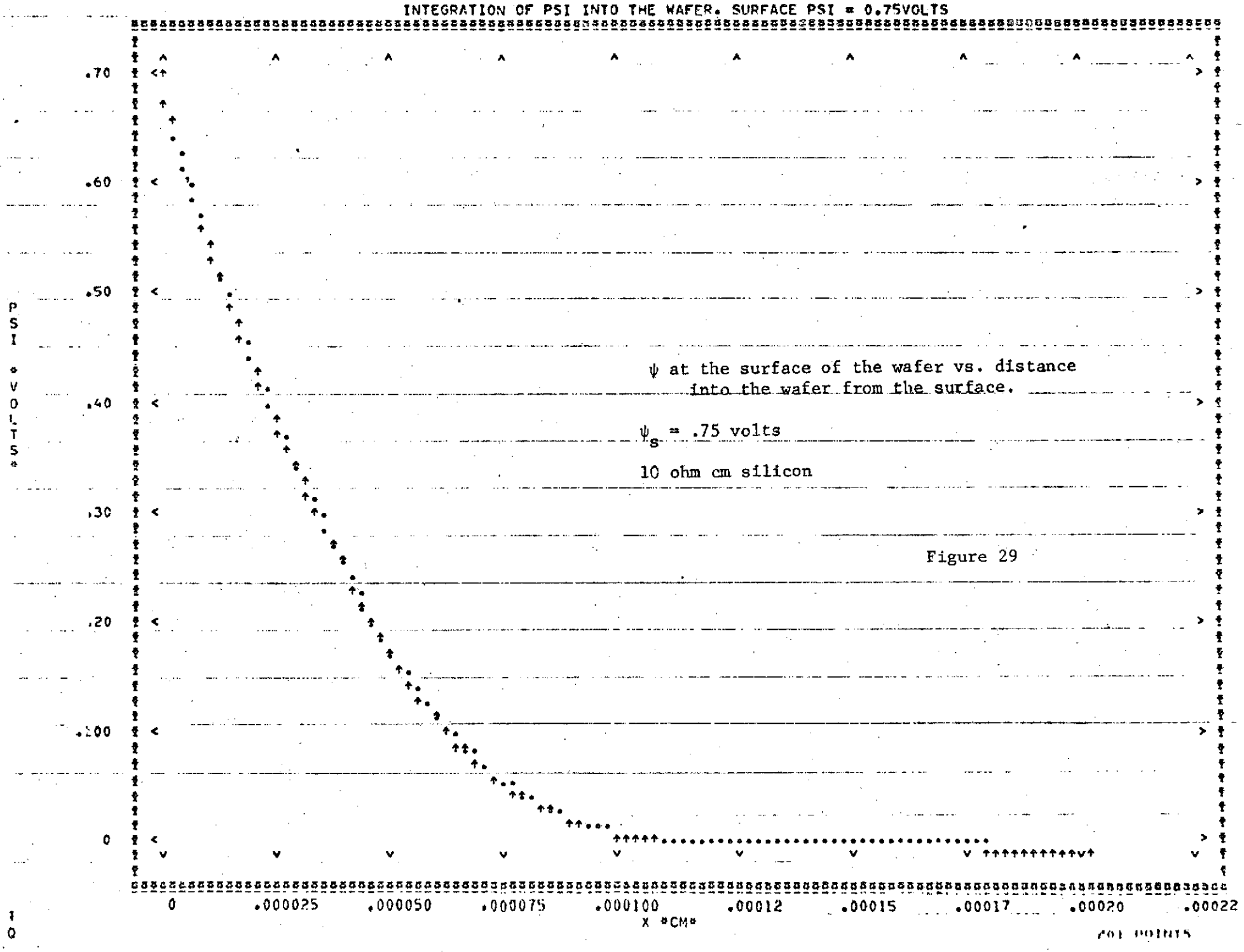
INTEGRATION OF PSI INTO THE WAFER. SURFACE PSI = 0.75VOLTS
.70
.60
.50
.40
.30
.20
.100
0
PSI *VOLTS*
ψ at the surface of the wafer vs. distance into the wafer from the surface.
ψ_s = .75 volts
10 ohm cm silicon
0
.000025
.000050
.000075
.000100
.00012
.00015
.00017
.00020
.00022
X *CM*
101 POINTS

Figure 29

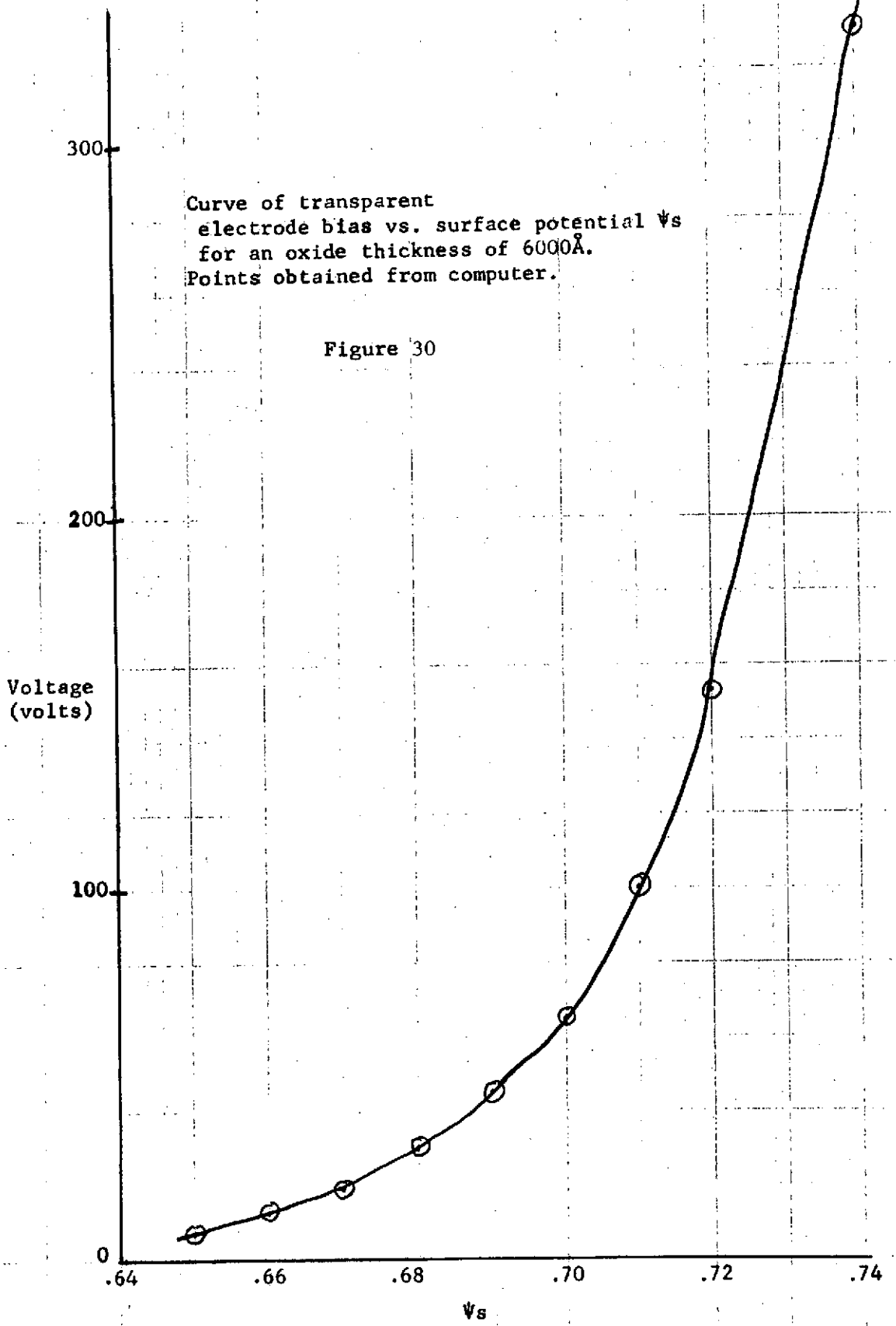

Curve of transparent electrode bias vs. surface potential Ψ_s for an oxide thickness of 6000Å. Points obtained from computer.

Figure 30

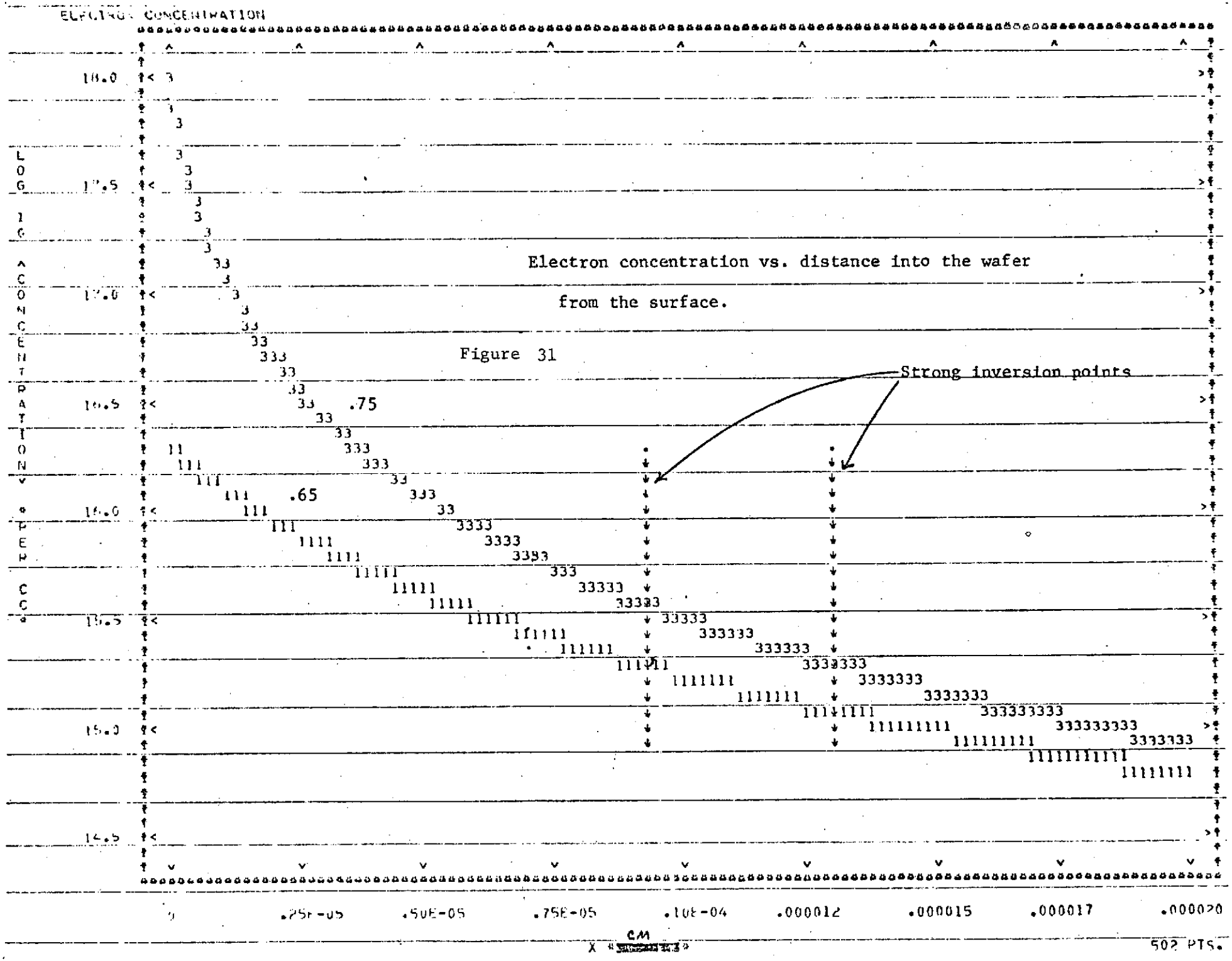

Electron concentration vs. distance into the wafer from the surface.

Figure 31

Strong inversion points

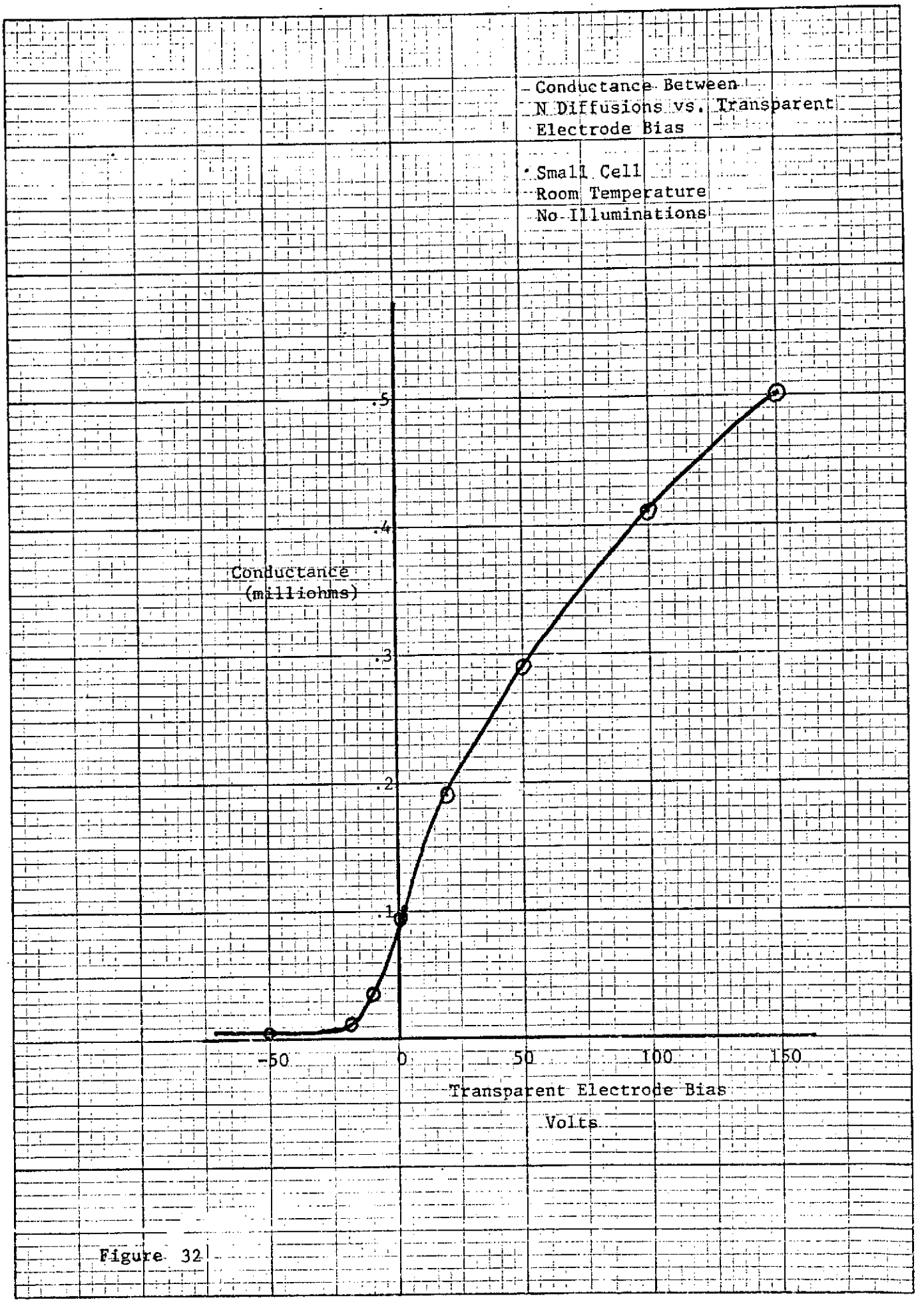

Figure 32

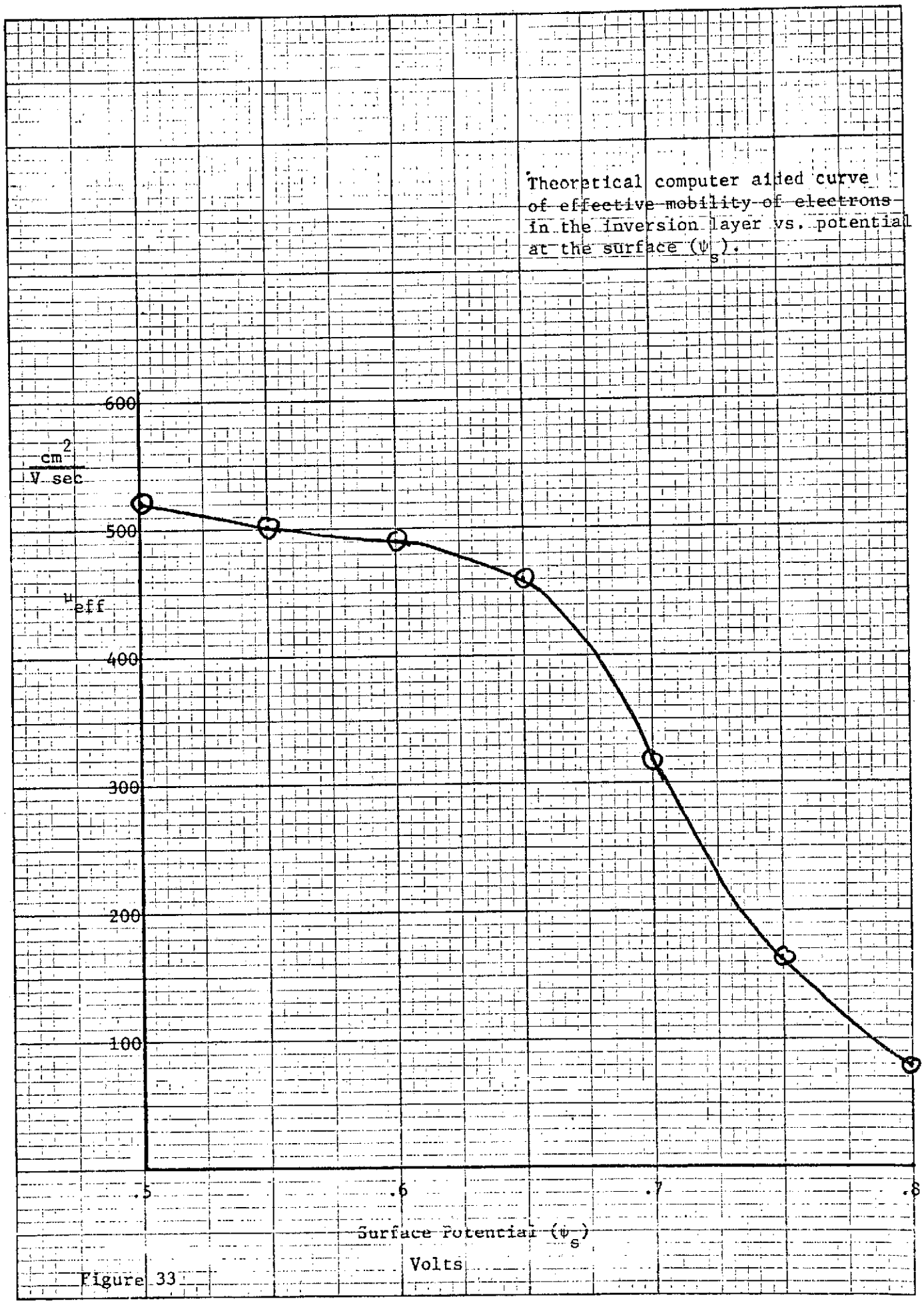

Figure 33

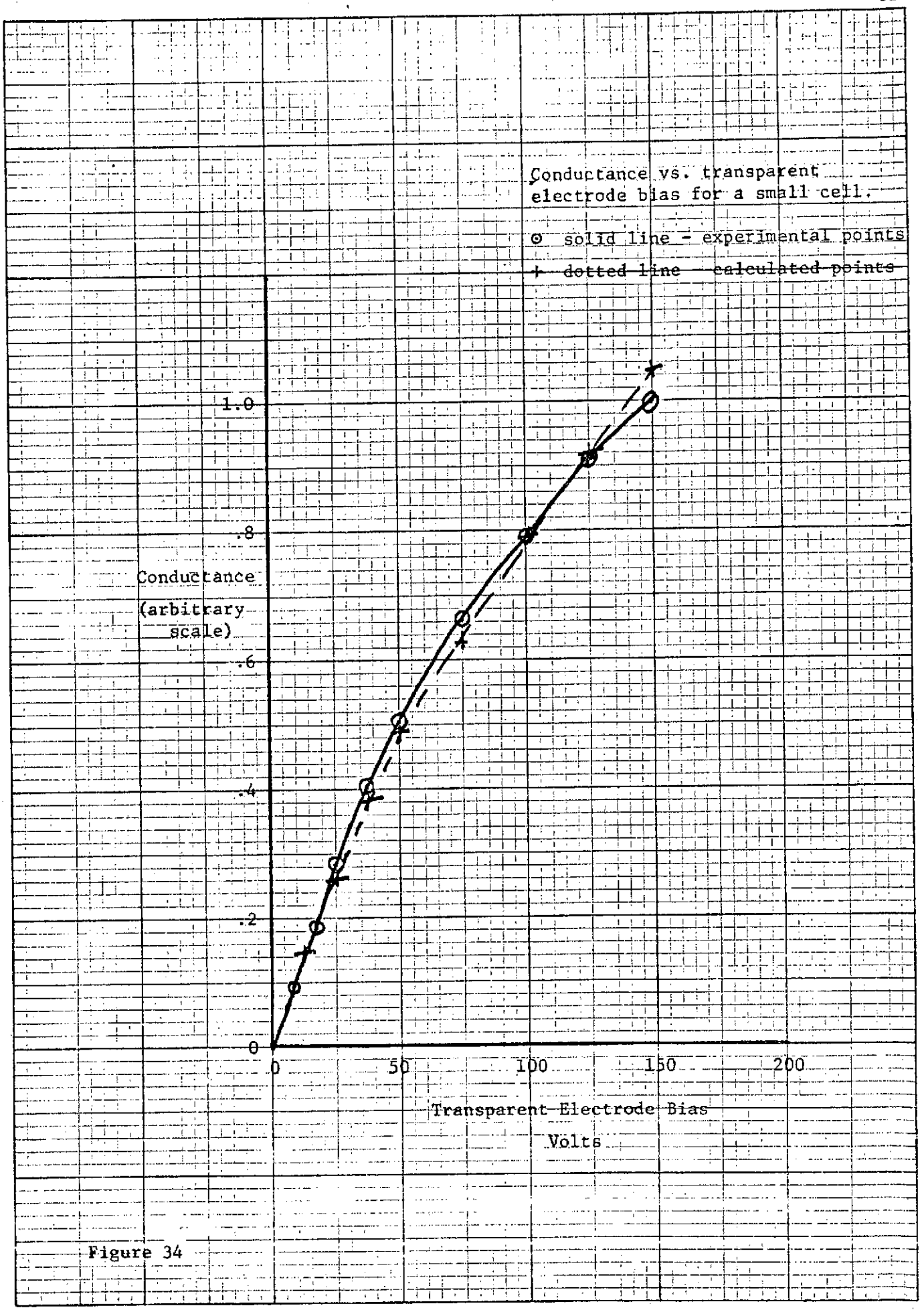

Figure 34

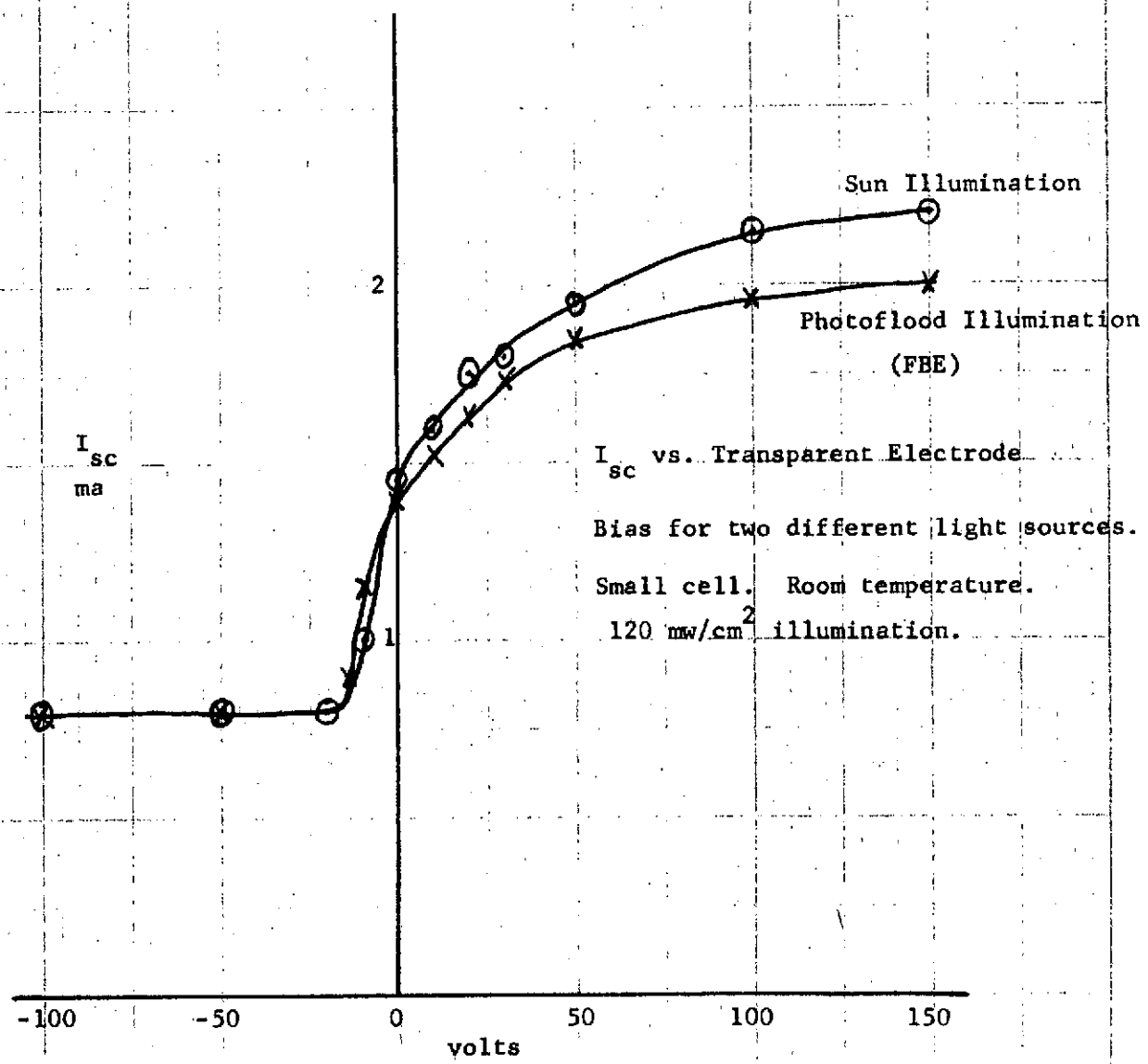
Sun Illumination
Photoflood Illumination
(FBE)
I_{sc} vs. Transparent Electrode Bias for two different light sources.
Small cell. Room temperature.
120 mw/cm^2 illumination.
I_{sc}
ma
2
1
-100
-50
0
50
100
150
volts
Transparent Electrode Bias

Figure 35

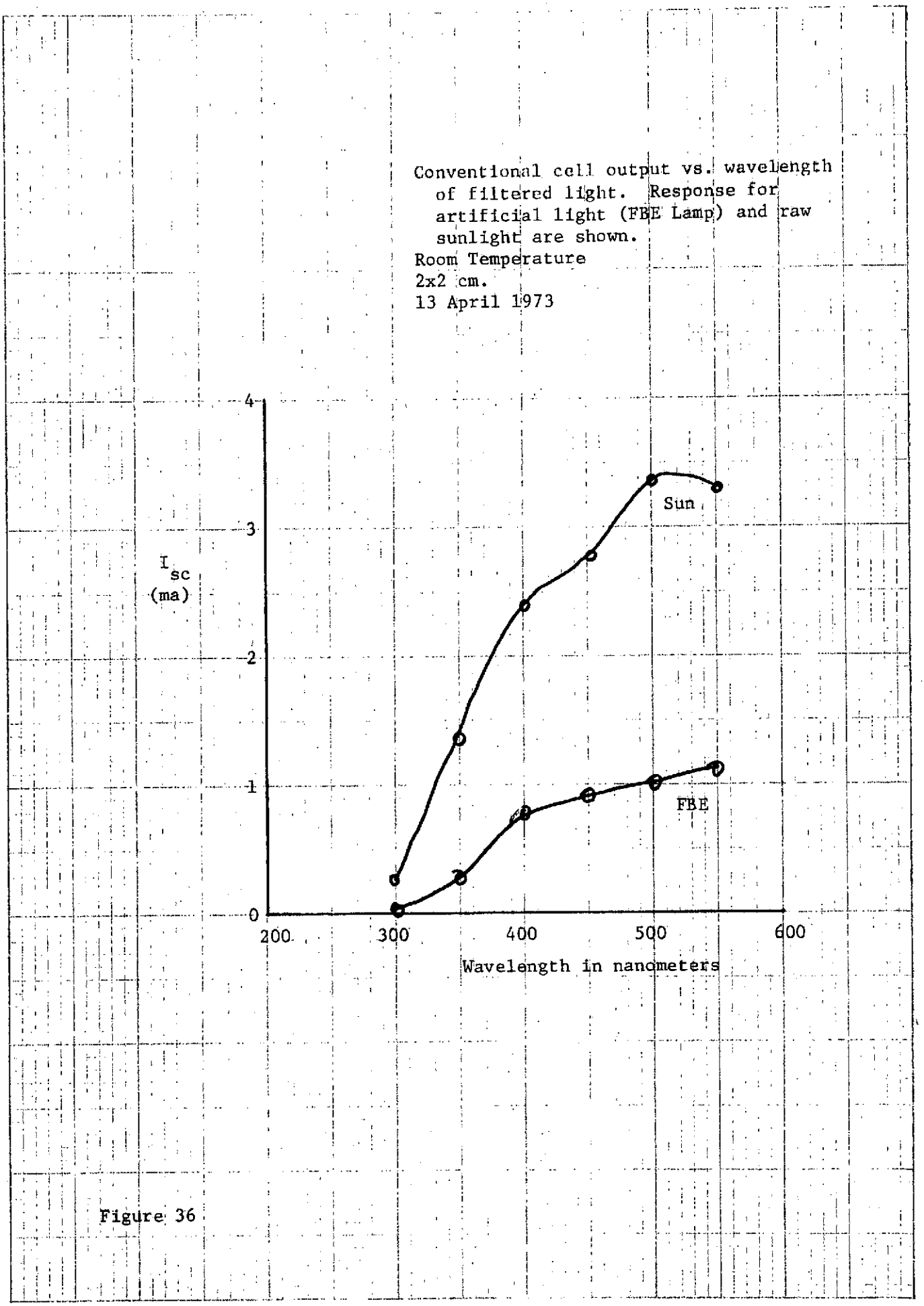
Conventional cell output vs. wavelength of filtered light. Response for artificial light (FBE Lamp) and raw sunlight are shown.
Room Temperature
2x2 cm.
13 April 1973
I_{sc} (ma)
0
1
2
3
4
200
300
400
500
600
Wavelength in nanometers
Sun
FBE

Figure 36

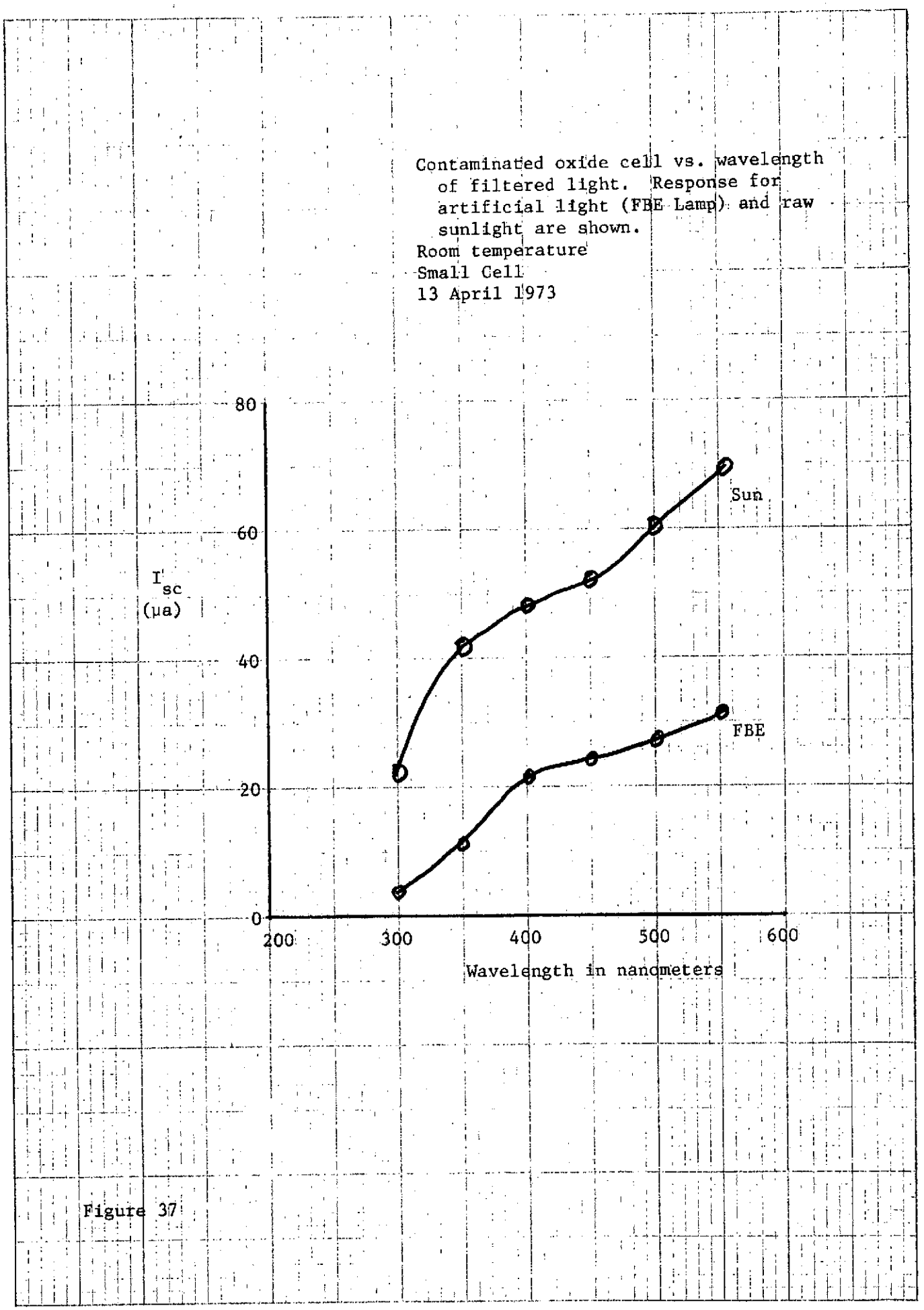
Contaminated oxide cell vs. wavelength of filtered light. Response for artificial light (FBE Lamp) and raw sunlight are shown.
Room temperature
Small Cell
13 April 1973
80
60
40
20
0
I_{sc} (μa)
Sun
FBE
200
300
400
500
600
Wavelength in nanometers

Figure 37

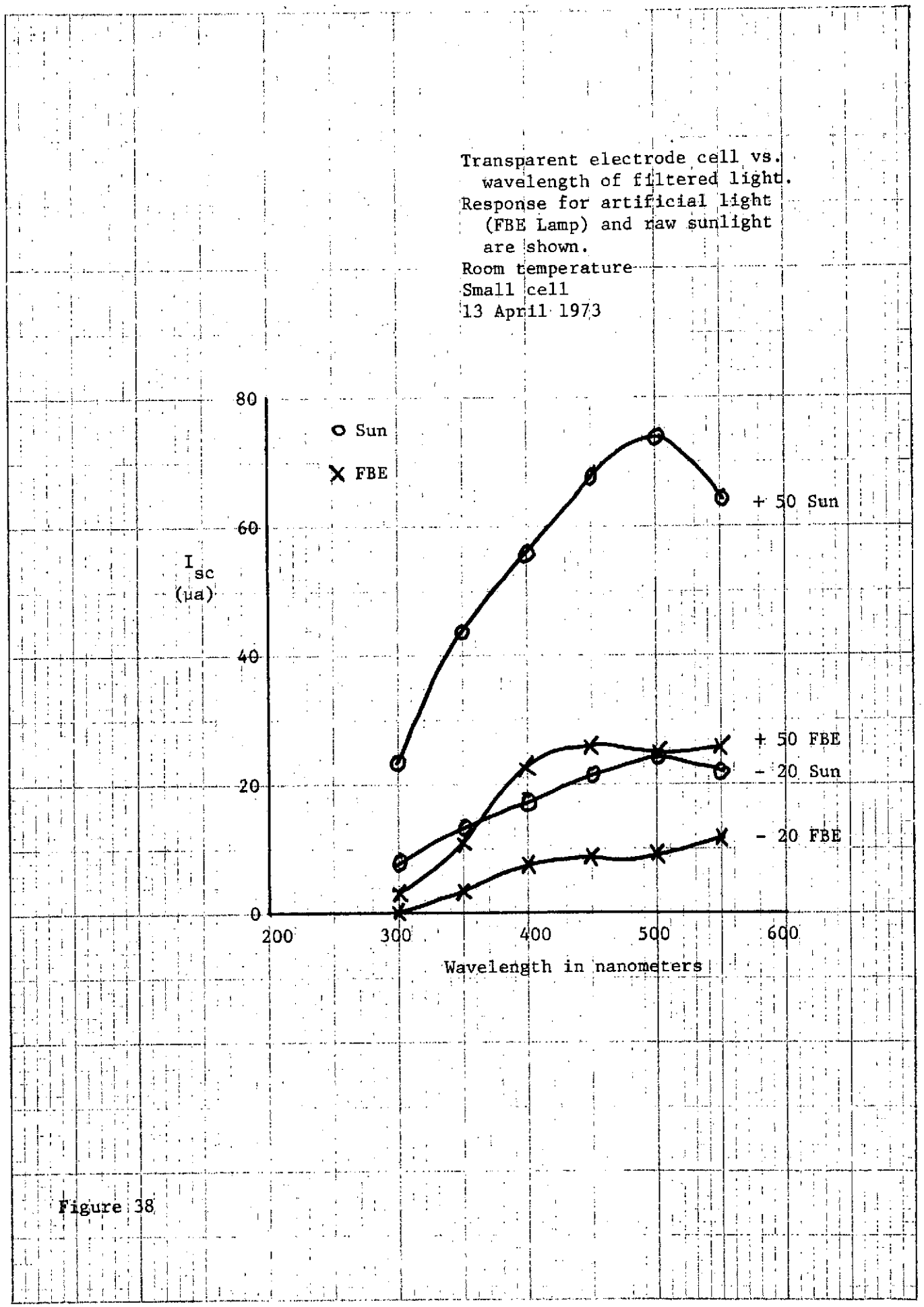
Transparent electrode cell vs.
wavelength of filtered light.
Response for artificial light
(FBE Lamp) and raw sunlight
are shown.
Room temperature
Small cell
13 April 1973
80
60
40
20
0
I_{sc}
(μa)
Sun
FBE
+ 50 Sun
+ 50 FBE
- 20 Sun
- 20 FBE
200
300
400
500
600
Wavelength in nanometers

Figure 38

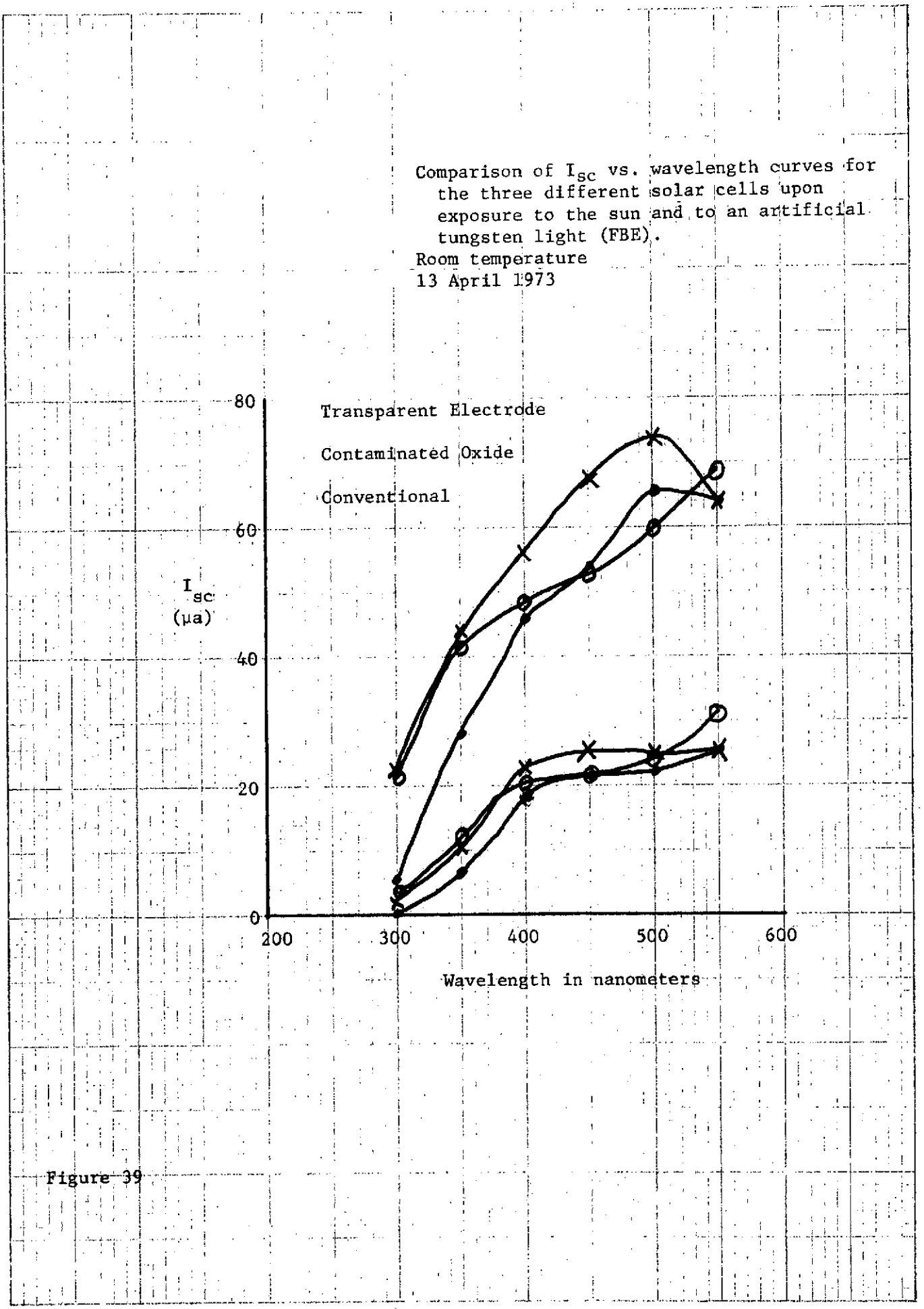
Comparison of I_{sc} vs. wavelength curves for the three different solar cells upon exposure to the sun and to an artificial tungsten light (FBE).
Room temperature
13 April 1973
Transparent Electrode
Contaminated Oxide
Conventional
I_{sc} (μa)
80
60
40
20
0
200
300
400
500
600
Wavelength in nanometers

Figure 39

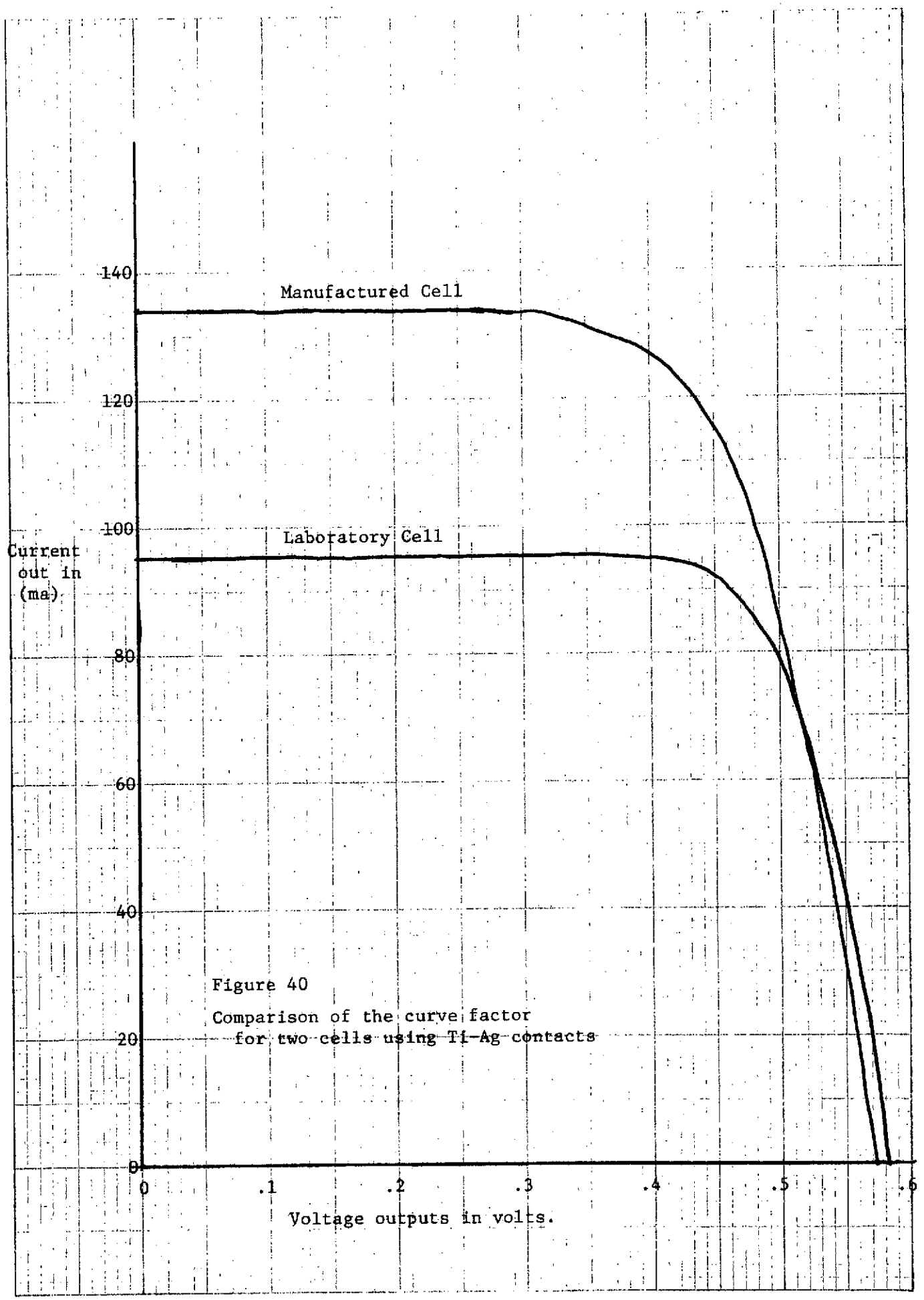

Figure 40

Comparison of the curve factor for two cells using Ti-Ag contacts

APPENDIX I

STANDARD PROCESSING SCHEDULE FOR TRANSPARENT ELECTRODE CELLS

1. Clean wafer with chromic and nitric acids, organic solvents and short HF dips.
2. Grow 6000 Å of steam oxide.
3. Using photoresist techniques, etch oxide for diffusion.
4. Phosphorus predeposition at 1050°C.
5. Strip all oxide.
6. Drive in n type dopant (phosphorus) and grow silicon oxide to desired thickness at 1100°C.
7. Deposit transparent oxide (SnO_2) in special furnace apparatus.
8. Photoresist and etch SnO_2 to SiO_2 surface.
9. Photoresist and etch SiO_2 to Si surface.
10. Evaporate metal on wafer. (Aluminize)
11. Photoresist and etch metal.
12. Sinter.
13. Test.